Line positions and intensities for the ν 2 /ν 4 bands of 5 isotopologues of germane near 11.5 μm

Cyril Richard, V. Boudon, A. Rizopoulos, J. Vander Auwera, F. Kwabia Tchana

▶ **To cite this version:**

Cyril Richard, V. Boudon, A. Rizopoulos, J. Vander Auwera, F. Kwabia Tchana. Line positions and intensities for the ν 2 /ν 4 bands of 5 isotopologues of germane near 11.5 μm. Journal of Quantitative Spectroscopy and Radiative Transfer, 2020, pp.107474. 10.1016/j.jqsrt.2020.107474 . hal-03076876

HAL Id: hal-03076876
https://hal.science/hal-03076876v1

Submitted on 16 Dec 2020

HAL is a multi-disciplinary open access archive for the deposit and dissemination of scientific research documents, whether they are published or not. The documents may come from teaching and research institutions in France or abroad, or from public or private research centers.

L'archive ouverte pluridisciplinaire **HAL**, est destinée au dépôt et à la diffusion de documents scientifiques de niveau recherche, publiés ou non, émanant des établissements d'enseignement et de recherche français ou étrangers, des laboratoires publics ou privés.

Graphical Abstract

Line positions and intensities for the ν_2/ν_4 bands of 5 isotopologues of germane near 11.5 μm

C. Richard, V. Boudon, A. Rizopoulos, J. Vander Auwera, F. Kwabia Tchana

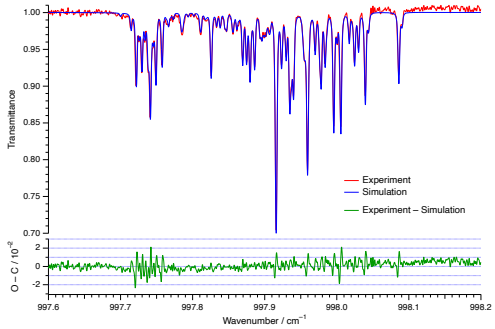

Highlights

Line positions and intensities for the ν_2/ν_4 bands of 5 isotopologues of germane near 11.5 μm

C. Richard, V. Boudon, A. Rizopoulos, J. Vander Auwera, F. Kwabia Tchana

- Complete line position and intensity analysis of the bending region of germane.
- Accurate determination of the Ge–H equilibrium bond length.
- Update of Germane Calculated Spectroscopic Database

Line positions and intensities for the ν_2/ν_4 bands of 5 isotopologues of germane near 11.5 μm

C. Richard[a,*], V. Boudon[a], A. Rizopoulos[b], J. Vander Auwera[b,1], F. Kwabia Tchana[c]

[a] *Laboratoire Interdisciplinaire Carnot de Bourgogne, UMR 6303 CNRS - Université Bourgogne Franche-Comté, 9 Av. A. Savary, BP 47870, F-21078 Dijon Cedex, France*
[b] *Spectroscopy, Quantum Chemistry and Atmospheric Remote Sensing (SQUARES), C.P. 160/09, Université Libre de Bruxelles, 50 avenue F.D. Roosevelt, B-1050 Brussels, Belgium*
[c] *Laboratoire Interuniversitaire des Systèmes Atmosphériques (LISA), UMR CNRS 7583, Université de Paris, Université Paris-Est Créteil, Institut Pierre-Simon Laplace, 61 avenue du Général de Gaulle, 94010 Créteil Cedex, France*

Abstract

Germane is a tetrahedral molecule found in trace abundance in giant gas planets like Jupiter and Saturn. We have recently provided a database of calculated lines of the stretching fundamental bands in the 2100 cm^{-1} region that is of high interest for planetology (https://vamdc.icb.cnrs.fr/PHP/GeH4.php). It is now necessary to study many rovibrational levels, including the lowest ones, in order to access the hot bands and thus to improve the model of the spectral region of interest for Jupiter, especially in the framework of the ongoing Juno mission. We present here a complete analysis and modeling of line positions and intensities in the ν_2/ν_4 bending dyad region near 900 cm^{-1} for all five germane isotopologues in natural abundance. Thanks to the high symmetry of the molecule, we use the tensorial formalism and group theory methods developed in the Dijon group, that allows us to provide a set of effective Hamiltonian and dipole parameters. The present study also leads to a refined value of the Ge–H equilibrium bond length of 1.51714(25) Å. Finally, new calculated germane lines were derived and injected in the GeCaSDa database.

Keywords:
Germane, High-Resolution Infrared Spectroscopy, Line positions, Line intensities, Tensorial Formalism

1. Introduction

The presence of germane in the atmosphere of giant planets is known since 1978 and the discovery of the molecule by Fink *et al.* [1] in the atmosphere of Jupiter in trace amount. In 2011, the Juno NASA space probe was launched toward the gas giant carrying the JIRAM

*Corresponding author
Email address: Cyril.Richard@u-bourgogne.fr (C. Richard)
[1] Senior research associate with the F.R.S.-FNRS, Belgium

(Jovian InfraRed Auroral Mapper) spectrometer, covering the large 1.993–5.014 μm range. Since 2016, Juno is orbiting Jupiter, recording data with an accuracy never reached before [2]. Accurate modeling of the GeH_4 infrared spectrum is now essential, in particular to allow the retrieval of other tropospheric species. In 2018, we have presented the first complete analysis and modeling of line positions and intensities in the strongly absorbing ν_1/ν_3 stretching dyad region near 2100 cm^{-1}, for all five germane isotopologues in natural abundance [3]. This study was recently used by Grassi *et al.* [4] in the analysis of the IR spectro-imager data leading to the creation of latitudinal profiles.

The introduction of our previous paper [3] presented a review of the different spectroscopic analyses conducted by other groups. Since that publication, we can additionally cite the very recent works of Ulenikov *et al.* [5, 6] about the analysis of this same bending dyad and of some hot bands in the 1100–1350 cm^{-1} region.

The present work constitutes a complete line position and intensity investigation of the bending region of germane between 715 and 1100 cm^{-1}. Although this region has not the same interest in planetology as the bands analyzed in our previous work, their modeling is an important step in the characterization of hot bands. This study allows us to fit effective Hamiltonian for $v_2 = 1$ and $v_4 = 1$ states. The ν_2 and ν_4 fundamental bands could be analyzed as an interacting dyad for the five isotopologues that are present in natural abundance: $^{70}GeH_4$ (21.23%), $^{72}GeH_4$ (27.66%), $^{73}GeH_4$ (7.73%), $^{74}GeH_4$ (35.94%) and $^{76}GeH_4$ (7.44%). We could also perform the fit of the effective dipole moment parameters for these two bands, leading to absolute line intensity predictions. Section 2 details the experimental method, while Section 3 focuses on the theoretical model developed in Dijon. Section 4 presents the line intensity measurements. Then, Section 5 presents and discusses the results of our analyses. The present data also allowed us to determine a new accurate value of the Ge–H equilibrium bond length.

2. Experimental details

Ten absorption spectra of germane (GeH_4) have been recorded in the range from 675 to 1210 cm^{-1} using the high-resolution Fourier transform spectrometer (FTS) Bruker IFS125HR located at the LISA facility in Créteil. The instrument was equipped with a silicon carbide Globar source, a KBr/Ge beamsplitter and an optimized home-made MCT detector developed at the AILES beamline [7], used in conjunction with two bandpass optical filters ($675 - 960$ and $810 - 1210$ cm^{-1}) to improve the signal-to-noise ratio (S/N). The FTS was continuously evacuated below 7 Pa by a dry pump to minimize absorption by atmospheric gases. The diameter of the entrance aperture of the spectrometer was set to 1.5 mm, to maximize the intensity of IR radiation falling onto the detector without saturation or loss of spectral resolution. Interferograms were recorded with a 40 kHz scanner frequency and a maximum optical path difference (MOPD) of 473.68 cm. According to the Bruker definition (resolution = 0.9 / MOPD), this corresponds to a resolution of 0.0019 cm^{-1}. The spectra were obtained by Fourier transformation of the interferograms using a Mertz phase correction, 1 cm^{-1} phase resolution, a zero-filling factor of 2 and no apodization (boxcar option).

Germane 5.0 (99.999 % stated purity) was purchased from Linde Gas and used without further purification. For all the measurements, a small cryogenic cell (5.10 ± 0.01 cm path length) made of stainless steel to minimize adsorption and corrosion issues, fitted with 9.5 mm diameter, 0.4 mm thick, wedged diamond windows (E6, Netherlands) and housed inside the sample compartment of the Bruker IFS125HR spectrometer, was used. A detailed description of the cell is given in Ref. [8]. The sample pressure in the cell was measured using calibrated MKS Baratron capacitance manometers models 627D (2 and 100 torr full scale) and 628 D (10 torr full scale), characterized by a stated reading accuracy of 0.12 %. Taking into account the uncertainty arising from small variations of the pressure during the recording (~ 0.35 %), we estimated the measurement uncertainty on the pressure to be equal to 0.5 %. All the spectra were recorded at a stabilized room temperature of 300 ± 1 K.

The following procedure was used to record the spectra. A background spectrum was first collected while the cell was being continuously evacuated. It was recorded at the same resolution as the sample spectra to ensure proper removal of the water vapor absorption lines and of the weak channeling generated by the wedged cell windows. The infrared gas cell was then passivated several times with the GeH_4 sample. Finally, spectra were recorded for ten different sample pressures of germane. The ten pressures chosen and the number of interferograms recorded and averaged to yield the corresponding spectra are listed in Table 1. All the sample spectra were ratioed against the empty cell background spectrum, and interpolated 4 times. The root mean square (RMS) S/N ratio in the ratioed spectra ranged between 270 and 750. For line position analysis, spectra S2, S4 and S7 were used and were calibrated by matching the measured positions of 32 lines of OCS observed in the 800–1000 cm^{-1} spectral region to reference wavenumbers available in HITRAN [9] with a RMS deviation of 0.0002 cm^{-1}. Figs 1 and 2 present an overview of the ν_4 region for 3 of the spectra recorded and the $R(4)$ manifold of the ν_4 band of the five isotopologues studied in the present work, respectively.

3. Theoretical model

As already mentioned in our previous work [3], germane is a tetrahedral spherical top molecule with T_d point group symmetry at equilibrium and possesses four normal modes of vibration. In this study we only focus on the doubly-degenerate mode with E symmetry, ν_2, and the triply-degenerate mode with F_2 symmetry, ν_4. They interact and form the ν_2/ν_4 bending dyad region and are respectively and approximately centered at 930 cm^{-1} and 820 cm^{-1}.

3.1. Effective Hamiltonian operator

Due to the high symmetry of the molecule, we use the tensorial formalism and group theory methods developed in the Dijon group [10, 11]. Let us just recall briefly the principles of this model.

We are here considering an XY_4 molecule for which the vibrational levels can be grouped into a series of polyads named P_k with $k = 0, \ldots, n$, $P_{k=0}$ being the ground state (GS). The

Hamiltonian operator is written as follows (assuming that some perturbative treatment such as a contact transformation [12] has been performed to eliminate inter-polyad interactions):

$$\mathcal{H} = \mathcal{H}_{\{P_0 \equiv GS\}} + \mathcal{H}_{\{P_1\}} + \ldots + \mathcal{H}_{\{P_k\}} + \ldots + \mathcal{H}_{\{P_{n-1}\}} + \mathcal{H}_{\{P_n\}}. \tag{1}$$

where the different $\mathcal{H}_{\{P_k\}}$ terms are expressed in the following form:

$$\mathcal{H}_{\{P_k\}} = \sum_{\text{all indexes}} t^{\Omega(K,n\Gamma)\Gamma_v\Gamma'_v}_{\{s\}\{s'\}} \beta \left[{}^{\varepsilon}V^{\Omega_v(\Gamma_v\Gamma'_v)\Gamma}_{\{s\}\{s'\}} \otimes R^{\Omega(K,n\Gamma)} \right]^{(A_1)}. \tag{2}$$

In this equation, the $t^{\Omega(K,n\Gamma)\Gamma v\Gamma' v}_{\{s\}\{s'\}}$ are the parameters to be determined, while ${}^{\varepsilon}V^{\Omega_v(\Gamma_v\Gamma'_v)\Gamma}_{\{s\}\{s'\}}$ and $\mathrm{R}^{\Omega(K,n\Gamma)}$ are vibrational and rotational operators, respectively. For each term, Ω_v and Ω represent the degree in elementary vibrational operators (creation a^+ and annihilation a operators), and rotational operators (components J_x, J_y and J_z of the angular momentum), respectively. $\varepsilon = (-1)^{\Omega}$ is the parity under time reversal. β is a factor that allows the scalar terms (terms with $\Gamma = A_1$, the totally symmetric irreducible representation of T_d) to match the "usual" contributions like $B_0 J^2$, *etc*. The order of each individual term is defined as $\Omega + \Omega_v - 2$. We deal with the effective Hamiltonians which are obtained, for a given polyad P_k, by the projection of H on the P_n Hilbert subspace:

$$\begin{aligned} \widetilde{H}^{<P_n>} &= P^{<P_n>}\mathcal{H}P^{<P_n>} \\ &= H^{<P_n>}_{\{\mathrm{GS}\}} + H^{<P_n>}_{\{P_1\}} + \ldots + H^{<P_n>}_{\{P_k\}} + \ldots + H^{<P_n>}_{\{P_{n-1}\}} + H^{<P_n>}_{\{P_n\}}. \end{aligned} \tag{3}$$

In the case we are interested in, ν_2 transitions are clearly visible while this band is "forbidden" in absorption. This, and the fact that ν_2 and ν_4 are close enough (≈ 100 cm^{-1}) imply an intensity borrowing by Coriolis coupling. Therefore we shall treat both bands as an interacting dyad, as this is often the case for tetrahedral XY_4 molecules [13, 14, 15].

We thus use the following effective Hamiltonians:

- The ground state effective Hamiltonian,

$$\widetilde{H}^{<\mathrm{GS}>} = H^{<\mathrm{GS}>}_{\{\mathrm{GS}\}}. \tag{4}$$

- The ν_2/ν_4 bending dyad effective Hamiltonian,

$$\widetilde{H}^{<\nu_2/\nu_4>} = H^{<\nu_2/\nu_4>}_{\{\mathrm{GS}\}} + H^{<\nu_2/\nu_4>}_{\{\nu_2/\nu_4\}}. \tag{5}$$

3.2. Effective dipole moment operator

In order to calculate transition absolute intensities, we also need to expand the effective dipole moment operator in a very similar way to what we did recently in the case of the RuO_4 [16] and SiF_4 [17] molecules. This operator, just as the effective Hamiltonian, is expanded as a sum of rovibrational operators, as detailed in Ref. [12]. In the case of the

ν_2/ν_4 bending dyad, it appears necessary to expand it up to order one plus a single second-order operator (with $K = 0$ for the rotational part) in the case of ν_4. This amounts to a total of four operators and thus to four associated parameters to be fitted using experimental line intensities:

$$\begin{aligned}\widetilde{\mu} \;=\;& \mu_2^1 \left(R^{1(1,0F_1)} \otimes {}^{-}V^{1(A_1E)E}_{\{\mathrm{GS}\}\{\nu_2\}}\right)^{(F_2)} \\ &+ \mu_4^0 \left(R^{0(0,0A_1)} \otimes {}^{+}V^{1(A_1F_2)F_2}_{\{\mathrm{GS}\}\{\nu_4\}}\right)^{(F_2)} \\ &+ \mu_4^1 \left(R^{1(1,0F_1)} \otimes {}^{-}V^{1(A_1F_2)F_2}_{\{\mathrm{GS}\}\{\nu_4\}}\right)^{(F_2)} \\ &+ \mu_4^2 \left(R^{2(2,0A_1)} \otimes {}^{+}V^{1(A_1F_2)F_2}_{\{\mathrm{GS}\}\{\nu_4\}}\right)^{(F_2)}, \end{aligned} \tag{6}$$

where we used a simplified notation for the effective parameters. Here, μ_4^0 is the dipole moment derivative relative to the q_4 normal mode coordinates and μ_4^1 is a rovibrational contribution that corresponds to the usual Herman-Wallis factor, while μ_4^2 is a second-order rovibrational correction and μ_2^1 is an induced rovibrational term for the ν_2 band (this term is induced into the effective dipole moment operator by the contact transformation that isolates the bending dyad; this has been previously explained in the case of methane, CH_4, see [18]). In Equation 6, the R and V symbols represent rotational and vibrational operators, just as in the case of the effective Hamiltonian operator; their construction is detailed in Refs. [12, 19]. In principle, there exist three other rovibrational operators at order two (with $K = 2$ for the rotational part), but these cannot be determined here (see Section 5.3) and are thus ignored.

3.3. Basis sets

The calculation of the effective Hamiltonian and effective dipole moment matrix elements are performed in the coupled rovibrational basis

$$\left|\left[\Psi_v^{(C_v)} \otimes \Psi_r^{(J,nC_r)}\right]_{\sigma}^{(C)}\right\rangle, \tag{7}$$

where $\Psi_r^{(J,nC_r)}$ is a rotational wavefunction with angular momentum J, rotational symmetry species C_r and multiplicity index n; $\Psi_v^{(C_v)}$ is a coupled vibrational basis set; C is the overall symmetry species ($C = C_v \otimes C_r$), with component σ. In the present case, $\Psi_v^{(C_v)}$ contains the relevant functions for the ν_2 and ν_4 normal modes of vibration (bending modes),

$$\left|\Psi_{v\ \sigma_v}^{(C_v)}\right\rangle = \left|(\Psi_{v_2}^{(l_2,n_2C_2)} \otimes \Psi_{v_3}^{(l_4,n_4C_4)})_{\sigma_v}^{(C_v)}\right\rangle, \tag{8}$$

with two contributions:

- For the doubly degenerate mode ν_2, we use a symmetrized doubly degenerate harmonic oscillator basis set denoted

$$\left|\psi_{v_2\ \sigma_2}^{(l_2,C_2)}\right\rangle = |v_2, l_2, C_2, \sigma_2\rangle, \tag{9}$$

  with $v_2 = l_2 = 1$ for the dyad under consideration, v_2 and l_2 being the usual vibrational angular momentum quantum numbers and $C_2 = E$.

- For the triply degenerate mode ν_4, we use a symmetrized triply degenerate harmonic oscillator basis set denoted

$$\left|\psi_{v_4\ \sigma_4}^{(l_4,n_4C_4)}\right\rangle = |v_4, l_4, n_4, C_4, \sigma_4\rangle\,, \tag{10}$$

  with $v_4 = l_4 = 1$ for the dyad under consideration, v_4 and l_4 being the usual vibrational angular momentum quantum numbers and $C_4 = F_2$, while n_4 is a multiplicity index.

The effective Hamiltonian matrix is diagonalized numerically, and this leads to eigenfunctions obtained from

$$\widetilde{H}\left|\Psi_\sigma^{(J,C,\alpha)}\right\rangle = E\left|\Psi_\sigma^{(J,C,\alpha)}\right\rangle, \tag{11}$$

where $\alpha = 1, 2, \ldots$ numbers functions with the same symmetry C in a given J block. This eigenbasis set can be expanded in terms of the initial rovibrational basis set (7) and is used to calculate the matrix elements (in Debye) of the Z component μ_Z of the effective dipole moment operator $\widetilde{\mu}$, in the laboratory-fixed frame. This μ_Z component is related to $\widetilde{\mu}$ from Equation (6) through Stone coefficients [20] and the direction cosines tensor as explained in Section 6.1. of Ref. [10]. The line intensity at temperature T for a transition at wavenumber $\widetilde{\nu}_{if}$ (in cm^{-1}) between an initial state i (with energy E_i, in Joules) and a final state f is then obtained through:

$$S_{if}(\mathrm{cm}^{-1}/(\mathrm{molecule\ cm}^{-2})) = \frac{1}{4\pi\varepsilon_0}\widetilde{\nu}_{if}\frac{8\pi^3}{3hcQ}e^{-\frac{E_i}{k_BT}}\left(1 - e^{-\frac{hc\widetilde{\nu}_{if}}{k_BT}}\right)R_{if}, \tag{12}$$

with

$$R_{if} = 3\sum_{\alpha_i,\alpha_f}\left|\left\langle\Psi_{\sigma_f}^{(J_i,C_i,\alpha_i)}\right|\mu_Z\left|\Psi_{\sigma_f}^{(J_f,C_f,\alpha_f)}\right\rangle\right|^2. \tag{13}$$

Q is the total partition function at temperature T, c the speed of light in vacuum, h Planck's constant and k_B Boltzmann's constant. The line strength S_{if} is expressed here in the so-called "HITRAN unit" [9].

4. Line intensity measurements

As was done in our previous contribution for germane [3], the line intensities were measured using a multi-spectrum fitting program developed in Brussels [21, 22]. This program adjusts a synthetic spectrum to each of any number of observed Fourier transform spectra, using a Levenberg-Marquardt non-linear least-squares fitting procedure. Each synthetic spectrum is the convolution of the molecular transmission spectrum with an instrument line shape function, calculated on a wavenumber scale interpolated 4 times with respect to that of the corresponding observed spectrum. The latter was estimated using the "extended ILS model" of the program *linefit* (version 14.5, [23]) relying on a few isolated strong lines of the ν_4 band of germane observed in the lowest pressure spectrum, interpolated 16 times and chosen because self broadening could be neglected. Neglecting its wavenumber dependence, the ILS thus determined was used during the multi-spectrum analysis of the spectra. The

profile of the molecular lines was modeled using a Voigt function [24], with Gaussian width always held fixed to the value calculated for the Doppler broadening. The measurements were carried out on small spectral intervals, ranging from 0.015 to 0.60 cm^{-1} and containing one to several lines. The background in each spectrum was modeled by a polynomial expansion up to the second order.

Of the 10 spectra recorded at pressures in the range $0.13 - 90$ torr, 7 were actually used. The measurements performed in the region of the ν_2 band involved the fitting of the self-broadening coefficients of lines stronger than about 2.0×10^{-23} $cm^{-1}/(molecule\ cm^{-2})$. The self broadening coefficients of the other lines were held fixed at 0.1 $cm^{-1}atm^{-1}$, a rough average of the self broadening coefficients measured in the ν_3 band [3]. The measurements performed for the P and R branches of the weaker ν_2 band mainly relied on the higher pressure spectra S4 to S7 (Table 1 and Fig. 3). Measurements for high J lines of the P branch also involved the lower pressure spectrum S3. Spectrum S7 was excluded from the analysis of the Q branch of the ν_2 band because the density of lines combined with pressure broadening led to rather significant overlapping of the lines, as illustrated in Fig. 4. The measurements performed in the region of the ν_2 band involved the fitting of the self-broadening coefficients of lines stronger than about 2.0×10^{-23} $cm^{-1}/(molecule\ cm^{-2})$. It was held fixed at 0.1 $cm^{-1}atm^{-1}$ for the other lines. Spectra corresponding to even higher pressures (30 to 90 torr, S8 to S10 in Table 1) were not used because the blending of lines was obviously more pronounced.

For both bands, the line intensity measurements involved the simultaneous fitting of the selected spectra. The required initial values of the positions and intensities (as well as the assignments) of lines belonging to the ν_4 and ν_2 bands of the 5 isotopologues of germane considered in the present work were generated relying on the results of the frequency analysis described in section 5.1. The high quality of the predictions proved to be particularly helpful in the analysis of the ν_2 band as the lines of the various isotopologues tend to appear close together, as illustrated in Fig. 5. The initial values of the positions and intensities of lines observed in the fitted spectral ranges but not predicted by the frequency analysis (most probably belonging to hot bands) were measured using the program `WSpectra` [25].

Figure 6 presents an example of the results of a fit. It involved 54 lines for a total of 83 fitted parameters. Signatures observed for the stronger lines in the residuals of the lower pressure spectrum may result from an imperfect modeling of the instrument line shape.

Altogether, 447/275, 489/309, 350/183, 512/325 and 355/171 line intensities have been measured for the ν_4/ν_2 bands of $^{70}GeH_4$, $^{72}GeH_4$, $^{73}GeH_4$, $^{74}GeH_4$ and $^{76}GeH_4$, respectively. They are associated with lines observed in the range from 753 to 1040 cm^{-1} and range from 6.1×10^{-24} to 1.2×10^{-19} $cm^{-1}/(molecule\ cm^{-2})$ at 300 K. Although self broadening coefficients have been determined in the present work, we prefer not to report them because of the rather low pressures involved and the fact that most of the lines are rather heavily blended leading to large uncertainties on the measured self broadening coefficients. As a result, no rotational dependence is observed for the 909 measured self broadening coefficients, with average equal to about 0.075 $cm^{-1}atm^{-1}$.

5. Analysis and discussion

5.1. Line positions

From Table 1, only experimental spectra S2, S4 and S7 were used in the line position analysis of the ν_2/ν_4 bending dyad. Because of the presence of five germane isotopologues in natural abundance, these spectra show a dense structure where many transitions are overlapped. We started the analysis of the most abundant isotopologue, $^{74}GeH_4$, using initial parameters taken from our work on the ν_1/ν_3 region and unpublished results that were included in the STDS (Spherical-Top Data System) package [26], part of the XTDS (eXtended spherical-Top Data System) software [27]. The calculation performed using these parameters led to a very good initial spectrum simulation that allowed to assign many transitions in P and R branches.

Assignments were made using the home made software SPVIEW (Spectrum-View) [27] in its new 2.0 beta version. The Q branch shows a higher transition density making assignments not straightforward. However, using a standard iterative Levenberg-Marquardt non-linear least squares fitting procedure, simulations and new assignment sets, we finally reached a total of 1394 assigned transitions, up to $J = 25$, with a set of 26 parameters and a root mean squares deviation of 4.86×10^{-4} cm^{-1}. Each line position was considered to have the same uncertainty of 10^{-3} cm^{-1}, which accounts for both peak position and global calibration uncertainties. GS parameters of the five isotopologues were fixed to their fitted values taken from the results of Ref. [3].

Once transition assignment was completed for the main isotopologue, we have used same parameters to investigate the less abundant isotopologues. For each isotopologue, only the band center was updated, trying to visually match most transitions. The same fit procedure as described above was then repeated. Parameters that could not be correctly fitted were fixed to the value of $^{74}GeH_4$.

The results and fit statistics for all five isotopologues are presented in Table 2. Seven parameters are used to define $v_2 = 1$ up to order 4, 13 for $v_4 = 1$ up to order 5 and six interactions parameters between states $v_2 = 1$ and $v_4 = 1$. The last column of the table allows to convert all these constant values to the "classical" notation. We obtained a very good fit whose root mean squares deviation is 4.58×10^{-4}cm^{-1}, 5.75×10^{-4}cm^{-1}, 3.10×10^{-4}cm^{-1}, 4.86×10^{-4}cm^{-1} and 3.03×10^{-4}cm^{-1} for each isotopologue ($^{70}GeH_4$, $^{72}GeH_4$, $^{73}GeH_4$, $^{74}GeH_4$, $^{76}GeH_4$), respectively.

In Ref. [5], Ulenikov *et al.* have presented comparable results, but using a different reduction (fix parameters are not the same). In our case we have significantly high number of assignments up to higher J values.

Figure 7 presents the fit residuals for line positions. Some polynomial deviation seems to appear in the ν_4 region (below 900 cm^{-1}). This may correspond to some higher order contributions to the effective Hamiltonian that we could not fit here. But the residuals remain very small, anyway.

Figure 8 shows the reduced energy levels in the case of $^{74}GeH_4$, defined by

$$\widetilde{\nu}_{\rm red} \;=\; \widetilde{\nu} - \sum_{\Omega} t^{\Omega(0,0A_1)A_1A_1}_{\{\rm GS\}\{\rm GS\}} (J(J+1))^{\Omega/2}$$

$$= \widetilde{\nu} - B_0 J(J+1) + D_0 J^2(J+1)^2 - \ldots, \tag{14}$$

where B_0, D_0, ... are ground state values, *i.e.* we subtract the dominant scalar polynomial terms in order to enhance levels splittings due to molecular symmetry. The colors illustrate the mixings due to the interaction between the two vibrational levels. We give both the calculated and observed reduced energy levels. Observed levels are simply levels reached by assigned transitions which are included in the fit. This gives a good idea of the sampling of the energy spectrum. The four other isotopologues lead to a very similar picture. This figure allows to judge the quality of the simulation performed using the present effective Hamiltonian parameters, when extrapolating to unassigned J values.

In Ref. [28], we have studied the isotopic dependance of band centers and Coriolis-interaction parameters, using a simple model and the present values. More detail is given in Figure 2 of this reference.

5.2. Equilibrium bond length

The determination of the equilibrium bond length r_e of a spherical-top molecule (which is the unique geometrical parameter that defines its equilibrium structure) is possible if one knows the value of the rotational constant B_0 in the ground state and rotational constant differences in all the vibrational fundamental levels, say $\Delta B_i = B_i - B_0$ ($i = 1$ to 4), where B_i is the rotational constant in an excited state with $v_i = 1$ [29]. The formula giving B_e (equilibrium value) is [14]:

$$B_e = B_0 - \frac{1}{2} \sum_{i=1}^{4} d_i \Delta B_i, \tag{15}$$

where d_i is the normal mode degeneracy ($d_1 = 1$, $d_2 = 2$, $d_3 = d_4 = 3$). The equilibrium bond length is then [14]:

$$r_e = \sqrt{\frac{3h}{64\pi^2 c m_{\mathrm{H}} B_e}}, \tag{16}$$

h being Planck's constant, c the speed of light in vacuum and m_{H} the hydrogen atom mass, whose values are taken from Ref. [30]. The fitted parameters $B_0 = t_{\{0\}\{0\}}^{2(0,0A_1)A_1A_1}$ and $\Delta B_i = t_{\{i\}\{i\}}^{2(0,0A_1)\Gamma_v\Gamma_v}$ ($i = 1$ to 4) result from the line position fits in Table 2 of Ref. [3] and in the present work (see Table 2). Using these fitted values and their standard deviation and averaging over all 5 isotopologues, we get:

$$B_e = 2.72531(95)\ \mathrm{cm}^{-1}, \tag{17}$$

and thus:

$$r_e(\mathrm{GeH_4}) = 1.51710(27)\ \text{Å}. \tag{18}$$

It should be recalled that, within the Born-Oppenheimer approximation, structural parameters like r_e do not depend on the isotopologue.

Somewhat higher values can be found in rather old references. The *CRC Handbook of Chemistry and Physics* [31] reports an experimental value $r_e = 1.5251$ Å, while Yu *et al.*

obtain a theoretical *ab initio* value r_e = 1.5358 Å [32]. However, in our previous work on $^{70}GeD_4$ [33], we reported r_e = 1.5173(1) Å, which is fully consistent with the present determination. Thus, going back to this Ref. [33], we can take again parameter values from its Tables 1 to 3 and include the accurate $^{70}GeD_4$ value in our average calculation, leading finally to:

$$r_e(GeH_4, GeD_4) = 1.51714(25) \text{ Å}. \quad (19)$$

Since the present study relies on highly accurate high-resolution spectroscopic data, it should be very reliable. Even considering a 3σ uncertainty (that would be 0.00075 Å), this rules out the previous higher values from the literature that we mentioned above. The value presented here can serve as a benchmark for new quantum chemistry calculations.

5.3. Line intensities

As explained in Section 4, the line positions and relative intensities prediction resulting from the effective Hamiltonian fit in Section 5.1 were useful for the measurements of absolute line intensities. By comparison with the theoretical predictions of line positions, this made possible the assignment of these lines for an intensity fit. We could then perform, for each isotopologue, a fit of the four effective dipole moment parameters up to order 2 that we described in Section 3.2 (as already mentioned, other operators at order two cannot be fitted and are ignored here). In this fit we consider only lines for which the relative observed minus calculated difference is bellow 10 %. This constitutes an extended intensity analysis in the bending dyad of germane, using several hundreds of intensity data for each isotopologue.

The resulting effective dipole moment parameters and fit statistics are displayed in Table 3. We get a very satisfactory result, with a relative standard deviation below 4 %, for all isotopologues.

We can compare these results with the recent work of Ulenikov *et al.* [5]. For each isotopologue we have used around twice more assigned lines and higher J values by two or three units. We notice that we get different values as well as a much smaller isotopic dependance for the dipole parameters of order 1 and 2.

Figure 9 displays the intensities for assigned lines, as well as the fit residuals for line intensities, for all five isotopologues. Figure 10 shows a simulation of the five germane isotopologues in natural abundance using the parameters derived from the fits in position and intensity discussed above. Figures 11 and 12 show a comparison and the difference between the experimental and simulated spectra (obtained using the effective Hamiltonian and dipole moment parameters fitted in this study) for the ν_4 region and for a small part of the ν_2 region, respectively.

6. GeCaSDa database update

We have updated the GeCaSDa database [34] by using an polyad scheme adapted to the ν_2/ν_4 bending dyad. The first scheme that was defined previously is dedicated to the ν_1/ν_3 fundamental bands and the second and new one to the present analysis. The complete database is illustrated in Table 4, where P_0 is the ground state and P_1 contains the fundamental levels ($v_1 = 1$ and $v_3 = 1$ for the first scheme and $v_2 = 1$ and $v_4 = 1$ for the second

one). An amount of 28 486 new transitions have been included in the database increasing to 60 878 the total number of lines. The calculated data are accessible either through our website at `http://vamdc.icb.cnrs.fr/PHP/gecasda.php` or on the VAMDC portal at `https://portal.vamdc.eu/vamdc_portal`. Our webpage allows to plot the data and download two sorts of file formats: the line by line list is given following the HITRAN 2004 format [35], while cross section is a simple 2-column flat file. An overview of the GeCaSDa database is displayed Figure 13, as downloadable from our website.

7. Conclusion

We have presented here a complete high-resolution study of both line positions and absolute line intensities of the ν_2/ν_4 bending dyad of germane, for its five isotopologues in natural abundance. We could determine accurate effective Hamiltonian and dipole moment parameters thanks to a series of high-quality infrared spectra. An accurate value of the Ge–H bond length has been derived. New calculated quantitative line lists have been derived and added to the GeCaSDa database [34], available form the VAMDC portal [36, 37, 38, 39]. These data will also be provided to the other public spectroscopic databases [9, 40].

Lines lists with assignments for line positions and line intensities are provided as supplementary material for this paper.

Although the bending dyad region is not the one used for the planetological detection of germane, the two low-lying vibrational levels which are characterized here are the main source of the hot bands in the ν_1/ν_3 stretching region, like $\nu_3 + \nu_2 - \nu_2$, $\nu_3 + \nu_4 - \nu_4$, *etc.* The present results are thus an essential first step towards the simulation of such hot bands of planetological interest. The next step will be the study of the upper states of these hot bands, through the analysis of combination bands like $\nu_3 + \nu_2$, $\nu_3 + \nu_4$, ...

Acknowledgments

This work was supported by the French National program LEFE "Les Enveloppes Fluides et l'Environnement" through the "MEANSPECFORUM" project.

References

[1] U. Fink, H. P. Larson, R. R. Treffers, Germane in the atmosphere of Jupiter, Icarus 34 (1978) 344–354.

[2] A. Adriani, A. Bracco, D. Grassi, M. L. Moriconi, A. Mura, G. Orton, F. Altieri, A. Ingersoll, S. K. Atreya, J. I. Lunine, A. Migliorini, R. Noschese, A. Cicchetti, R. Sordini, F. Tosi, G. Sindoni, C. Plainaki, B. M. Dinelli, D. Turrini, G. Filacchione, G. Piccioni, S. J. Bolton, Two-year observations of the Jupiter polar regions by JIRAM on board Juno, Journal of Geophysical Research: Planets 125 (2020) e2019JE006098.

[3] V. Boudon, T. Grigoryan, F. Philipot, C. Richard, F. Kwabia Tchana, L. Manceron, A. Rizopoulos, J. Vander Auwera, T. Encrenaz, Line positions and intensities for the ν_3 band of 5 isotopologues of germane for planetary applications, J. Quant. Spectrosc. Radiat. Transfer 205 (2018) 174–183.

[4] D. Grassi, A. Adriani, A. Mura, S. Atreya, L. Fletcher, J. Lunine, G. Orton, S. Bolton, C. Plainaki, G. Sindoni, et al., On the spatial distribution of minor species in Jupiter's troposphere as inferred from Juno JIRAM data, Journal of Geophysical Research: Planets 125 (2020) e2019JE006206.

[5] O. N. Ulenikov, O. V. Gromova, E. S. Bekhtereva, N. I. Raspopova, A. V. Kuznetsov, C. Sydow, S. Bauerecker, High resolution analysis of GeH_4 in the dyad region: Ro-vibration energy structure of $^{70}GeH_4$ and line strengths of $^{M}GeH_4$ ($M = 70, 72, 73, 74, 76$), J. Quant. Spectrosc. Radiat. Transfer 236 (2019) 106581.

[6] O. N. Ulenikov, O. V. Gromova, E. S. Bekhtereva, N. I. Raspopova, K. Berezkin, C. Sydow, S. Bauerecker, Line strengths anlysis of germane in the $1100 - 1350$ cm^{-1} region: the $\nu_1 - \nu_4$, $\nu_3 - \nu_4$, $\nu_3 - \nu_2$ and $\nu_1 - \nu_2$ "hot" bands of $^{M}GeH_4$ ($M = 70, 72, 73, 74, 76$), J. Quant. Spectrosc. Radiat. Transfer 242 (2020) 106755.

[7] M. Faye, M. Bordessoule, B. Kanouté, J.-B. Brubach, P. Roy, L. Manceron, Improved mid infrared detector for high spectral or spatial resolution and synchrotron radiation use, Rev. Sci. Inst. 87 (2016) 063119.

[8] A. Anantharajah, F. K. Tchana, L. Manceron, M. N. J.-M. Flaud, X. Landsheere, Integrated band intensities and absorption cross sections of phosgene (Cl_2CO) in the mid-infrared at 199, 250 and 300 K, J. Quant. Spectrosc. Radiat. Transfer 234 (2019) 71–77.

[9] I. E. Gordon, L. S. Rothman, C. Hill, R. V. Kochanova, Y. Tan, P. F. Bernath, M. Birk, V. Boudon, A. Campargue, K. V. Chance, B. J. Drouin, J.-M. Flaud, R. R. Gamache, J. T. Hodges, D. Jacquemart, V. I. Perevalov, A. Perrin, K. P. Shine, M.-A. H. Smith, J. Tennyson, G. C. Toon, H. Tran, V. G. Tyuterev, A. Barbe, A. Csaszar, M. V. Devi, T. Furtenbacher, J. J. Harrison, A. Jolly, T. Johnson, T. Karman, I. Kleiner, A. A. Kyuberis, J. Loos, O. M. Lyulin, S. T. Massie, S. N. Mikhailenko, N. Moazzen-Ahmadi, H. S. P. Müller, O. V. Naumenko, A. V. Nikitin, O. L. Polyansky, M. Rey, M. Rotger, S. Sharpe, K. Sung, E. Starikova, S. A. Tashkun, J. V. Auwera, G. Wagner, J. Wilzewski, P. Wcisło, S. Yu, E. J. Zak, The HITRAN2016 Molecular Spectroscopic Database, J. Quant. Spectrosc. Radiat. Transfer 203 (2017) 3–69.

[10] V. Boudon, J.-P. Champion, T. Gabard, M. Loëte, M. Rotger, C. Wenger, Spherical top theory and molecular spectra, in: M. Quack, F. Merkt (Eds.), Handbook of High Resolution Spectroscopy, Vol. 3, John Wiley & Sons, Ltd, Chichester, 2011, Ch. 39, pp. 1437–1460.

[11] C. Wenger, V. Boudon, M. Rotger, J. P. Sanzharov, J. P. Champion, XTDS and SPVIEW: Graphical tools for the analysis and simulation of high-resolution molecular spectra, Journal of Molecular Spectroscopy 251 (2008) 102–113.

[12] J.-P. Champion, M. Loëte, G. Pierre, Spherical top spectra, in: K. N. Rao, A. Weber (Eds.), Spectroscopy of the Earth's atmosphere and interstellar medium, Academic Press, San Diego, 1992, pp. 339–422.

[13] M. Loëte, Complete development of the dipole moment of tetrahedral molecules. Application to triply degenerate bands and to the dyad ν_2 and ν_4, Can. J. Phys. 61 (1983) 1242–1259.

[14] M. Louviot, V. Boudon, L. Manceron, P. Roy, D. Bermejo, R. Z. Martínez, High-resolution spectroscopy and structure of osmium tetroxide. A benchmark study on $^{192}OsO_4$, Inorg. Chem. 51 (2012) 10356–10365.

[15] S. Reymond-Laruinaz, M. Faye, V. Boudon, D. Doizi, L. Manceron, High-resolution infrared spectroscopy and analysis of the ν_2/ν_4 bending dyad of ruthenium tetroxide, J. Mol. Spectrosc. 336 (2017) 29–35.

[16] J. Vander Auwera, S. Reymond-Laruinaz, V. Boudon, D. Doizi, L. Manceron, Line intensity measurements and analysis in the ν_3 band of ruthenium tetroxide, J. Quant. Spectrosc. Radiat. Transfer 204 (2018) 103–111.

[17] V. Boudon, L. Manceron, C. Richard, High-resolution spectroscopy and analysis of the ν_3, ν_4 and $2\nu_4$ bands of SiF_4 in natural isotopic abundance, J. Quant. Spectrosc. Radiat. Transfer 253 (1999) 107114.

[18] M. Loëte, Développement complet du moment dipolaire des molécules tétraèdriques. Application aux bandes triplement dégénérées et à la diade ν_2 et ν_4, Can. J. Phys. 61 (1983) 1242–1259.

[19] V. Boudon, J.-P. Champion, T. Gabard, M. Loëte, M. Rotger, C. Wenger, Spherical top theory and molecular spectra, in: M. Quack, F. Merkt (Eds.), Handbook of High-Resolution Spectroscopy, Vol. 3, Wiley, Chichester, West Sussex, United Kingdom, 2011, pp. 1437–1460.

[20] A. J. Stone, Transformation between cartesian and spherical tensors, Mol. Phys. 29 (1975) 1461–1471.

[21] M. Tudorie, T. Foldes, A. Vandaele, J. V. Auwera, CO_2 pressure broadening and shift coefficients for the 1–0 band of HCl and DCl, J. Quant. Spectrosc. Radiat. Transfer 113 (2012) 1092–1101.
[22] L. Daneshvar, T. Foeldes, J. Buldyreva, J. V. Auwera, CO_2 pressure broadening and shift coefficients for the 1–0 band of HCl and DCl, J. Quant. Spectrosc. Radiat. Transfer 149 (2014) 258–274.
[23] F. Hase, T. Blumenstock, C. Paton-Walsh, Analysis of the instrumental line shape of high-resolution Fourier transform IR spectrometers with gas cell measurements and new retrieval software, Appl. Opt. 38 (1999) 3417–3422.
[24] R. J. Wells, Rapid approximation to the Voigt/Faddeeva function and its derivatives, J. Quant. Spectrosc. Radiat. Transfer 62 (1999) 29–48.
[25] M. R. Carleer, WSpectra: a Windows program to accurately measure the line intensities of high-resolution Fourier transform spectra, in: Remote sensing of clouds and the atmosphere V, Vol. 4168, SPIE, 2001, pp. 337–342.
[26] C. Wenger, J.-P. Champion, Spherical top data system (STDS) software for the simulation of spherical top spectra, J. Quant. Spectrosc. Radiat. Transfer 59 (1998) 471–480.
[27] C. Wenger, V. Boudon, M. Rotger, M. Sanzharov, J.-P. Champion, XTDS and SPVIEW: Graphical tools for the analysis and simulation of high-resolution molecular spectra, J. Mol. Spectrosc. 251 (2008) 102–113.
[28] M. Loëte, C. Richard, V. Boudon, Isotopic relations for tetrahedral and octahedral molecules, J. Mol. Struct. 1206 (2020) 127729.
[29] V. Boudon, J. L. Doménech, D. Bermejo, H. Willner, High-resolution Raman spectroscopy of the ν_1 region and Raman-Raman double resonance spectroscopy of the $2\nu_1 - \nu_1$ band of $^{32}SF_6$ and $^{34}SF_6$. Determination of the equilibrium bond length of sulfur hexafluoride, J. Mol. Spectrosc. 228 (2004) 392–400.
[30] E. R. Cohen, T. Cvitas, J. G. Frey, B. Holmström, K. Kuchitsi, R. Marquardt, I. Mills, F. Pavese, M. Quack, J. Stohner, H. L. Strauss, M. Takami, A. Thor, Quantities, Units and Symbols in physical chemistry, Third edition, IUPAC and Royal Society of Chemistry, RSC, Cambridge, 2007.
[31] D. R. Lide (Ed.), Handbook of Chemistry and Physics, 84th Edition, CRC Press, 2004.
[32] X. Yu, S.-M. Li, Z.-S. Li, C.-C. Sun, Direct *ab initio* dynamics studies of the reaction paths and rate constants of hydrogen atom with germane and silane, J. Phys. Chem. A 104 (2000) 9207–9212.
[33] G. Pierre, V. Boudon, E. B. Mkadmi, H. Bürger, D. Bermejo, R. Martínez, Study of the fundamental bands of $^{70}GeD_4$ by high-resolution Raman and infrared spectroscopy: First experimental determination of the equilibrium bond length of germane, J. Mol. Spectrosc. 216 (2002) 408–418.
[34] C. Richard, V. Boudon, M. Rotger, Calculated spectroscopic databases for the VAMDC portal: New molecules and improvements, J. Quant. Spectrosc. Radiat. Transfer 251 (2020) 107096.
[35] L. S. Rothman, I. E. Gordon, Y. Babikov, A. Barbe, D. C. Benner, P. E. Bernath, M. Birk, L. Bizzocchi, V. Boudon, L. R. Brown, A. Campargue, K. Chance, , E. A. Cohen, L. H. Coudert, V. M. Devi, S. Fally, B. J. Drouin, A. Fayt, J. M. Flaud, R. R. Gamache, J. J. Harrison, H. J.-M., C. Hill, J. T. Hodges, D. Jacquemart, A. Jolly, J. Lamouroux, R. Le Roy, G. Li, D. A. Long, O. M. Lyulin, C. J. Mackie, S. Massie, S. Mikhailenko, H. Müller, O. V. Naumenko, A. V. Nikitin, J. Orphal, V. Perevalov, E. R. Perrin A. andPolovtseva, C. Richard, M. A. H. Smith, E. Starikova, K. Sung, S. Tashkun, J. Tennyson, G. C. Toon, V. G. Tyuterev, G. Wagner, The HITRAN 2012 molecular spectroscopic database, J. Quant. Spectrosc. Radiat. Transfer 130 (2013) 4–50.
[36] M. L. Dubernet, V. Boudon, J. L. Culhane, M. S. Dimitrijevic, A. Z. Fazliez, C. Joblin, F. Kupka, G. Leto, P. L. Sidaner, P. A. Loboda, H. E. Mason, N. J. Mason, C. Mendoza, G. Mulas, T. J. Millar, L. A. Nuñez, V. I. Perevalov, N. Piskunov, Y. Ralchenko, G. Rixon, L. S. Rothman, E. Roueff, T. A. Ryabchikova, A. Ryabtsev, S. Sahal-Bréchot, B. Schmitt, S. Schlemmer, J. Tennyson, V. G. Tyuterev, N. A. Walton, V. Wakelam, C. J. Zeippen, Virtual Atomic and Molecular Data Centre, J. Quant. Spectrosc. Radiat. Transfer 111 (2010) 2151–2159.
[37] M. L. Dubernet, B. K. Antony, Y. A. Ba, Y. L. Babikov, K. Bartschat, V. Boudon, B. J. Braams, H.-K. Chung, F. Daniel, F. Delahaye, G. D. Zanna, J. de Urquijo, A. Domaracka, M. Doronin, B. J. Drouin, M. S. Dimitrijevic, C. P. Endres, E. Quintas-Sanchez, A. Z. Fazliev, S. V. Gagarin, I. E.

Gordon, U. Heiter, C. Hill, D. Jevremovic, C. Joblin, A. Kasprzak, E. Krishnakumar, G. Leto, P. A. Loboda, T. Louge, S. Maclot, B. P. Marinkovic, A. Markwick, T. Marquart, H. E. Mason, N. J. Mason, C. Mendoza, A. A. Mihajlov, T. J. Millar, N. Moreau, G. Mulas, G. Leto, Y. Pakhomov, P. Palmeri, S. Pancheshnyi, V. I. Perevalov, N. Piskunov, J. Postler, P. Gratier, P. Quinet, G. Rixon, Y. Ralchenko, Y.-J. Rhee, L. S. Rothman, E. Roueff, T. Ryabchikova, S. Sahal-Bréchot, P. Scheier, S. Schlemmer, B. Schmitt, E. Stempels, J. Tennyson, V. G. Tyuterev, V. Vujcic, V. Wakelam, N. A. Walton, O. Zatsarinny, C. J. Zeippen, C. M. Zwolf, the VAMDC Consortium, The Virtual Atomic and Molecular Data Centre (VAMDC) consortium for astrophysics, Journal of Physics B 49 (2016) 074003–1–074003–18.

[38] N. Moreau, C. M. Zwolf, Y. A. Ba, C. Richard, V. Boudon, M.-L. Dubernet, The VAMDC portal as a major enabler of atomic and molecular data citation, Galaxies 6 (2018) 105.

[39] D. Albert, B. K. Antony, Y. A. Ba, Y. L. Babikov, P. Bollard, V. Boudon, F. Delahaye, G. Del Zanna, M. S. Dimitrijević, B. J. Drouin, M.-L. Dubernet, F. Duensing, M. Emoto, C. P. Endres, A. Z. Fazliev, J.-M. Glorian, I. E. Gordon, P. Gratier, C. Hill, D. Jevremović, C. Joblin, D.-H. Kwon, R. V. Kochanov, E. Krishnakumar, G. Leto, P. A. Loboda, A. A. Lukashevskaya, O. M. Lyulin, B. P. Marinković, A. Markwick, T. Marquart, N. J. Mason, C. Mendoza, T. J. Millar, N. Moreau, S. V. Morozov, T. Möller, H. S. P. Müller, G. Mulas, I. Murakami, Y. Pakhomov, P. Palmeri, J. Penguen, V. I. Perevalov, N. Piskunov, J. Postler, A. I. Privezentsev, P. Quinet, Y. Ralchenko, Y.-J. Rhee, C. Richard, G. Rixon, L. S. Rothman, E. Roueff, T. Ryabchikova, S. Sahal-Bréchot, P. Scheier, P. Schilke, S. Schlemmer, K. W. Smith, B. Schmitt, I. Y. Skobelev, V. A. Srecković, E. Stempels, S. A. Tashkun, J. Tennyson, V. G. Tyuterev, C. Vastel, V. Vujčić, V. Wakelam, N. A. Walton, C. Zeippen, C. M. Zwölf, A decade with VAMDC: Results and ambitions, Atoms 8 (2020) 76.

[40] N. Jacquinet-Husson, R. Armante, N. A. Scott, A. Chedin, L. Crepeau, C. Boutammine, A. Bouhdaoui, C. Crevoisier, V. Capelle, C. Boonne, N. Poulet-Crovisier, A. Barbe, D. C. Benner, V. Boudon, L. R. Brown, J. Buldyreva, A. Campargue, L. H. Coudert, V. M. Devi, M. J. Down, B. J. Drouin, A. Fayt, C. Fittschen, J. M. Flaud, R. R. Gamache, J. J. Harrison, C. Hill, O. Hodnebrog, S. M. Hu, D. Jacquemart, A. Jolly, E. Jimenez, N. N. Lavrentieva, A. W. Liu, L. Lodi, O. M. Lyulin, S. T. Massie, S. Mikhailenko, H. S. P. Mueller, O. V. Naumenko, A. Nikitin, C. J. Nielsen, J. Orphal, V. I. Perevalov, A. Perrin, E. Polovtseva, A. Predoi-Cross, M. Rotger, A. A. Ruth, S. S. Yu, K. Sung, S. A. Tashkun, J. Tennyson, V. I. G. Tyuterev, J. V. Auwera, B. A. Voronin, A. Makie, The 2015 edition of the GEISA spectroscopic database, J. Mol. Spectrosc. 327 (2016) 31–72.

Figures

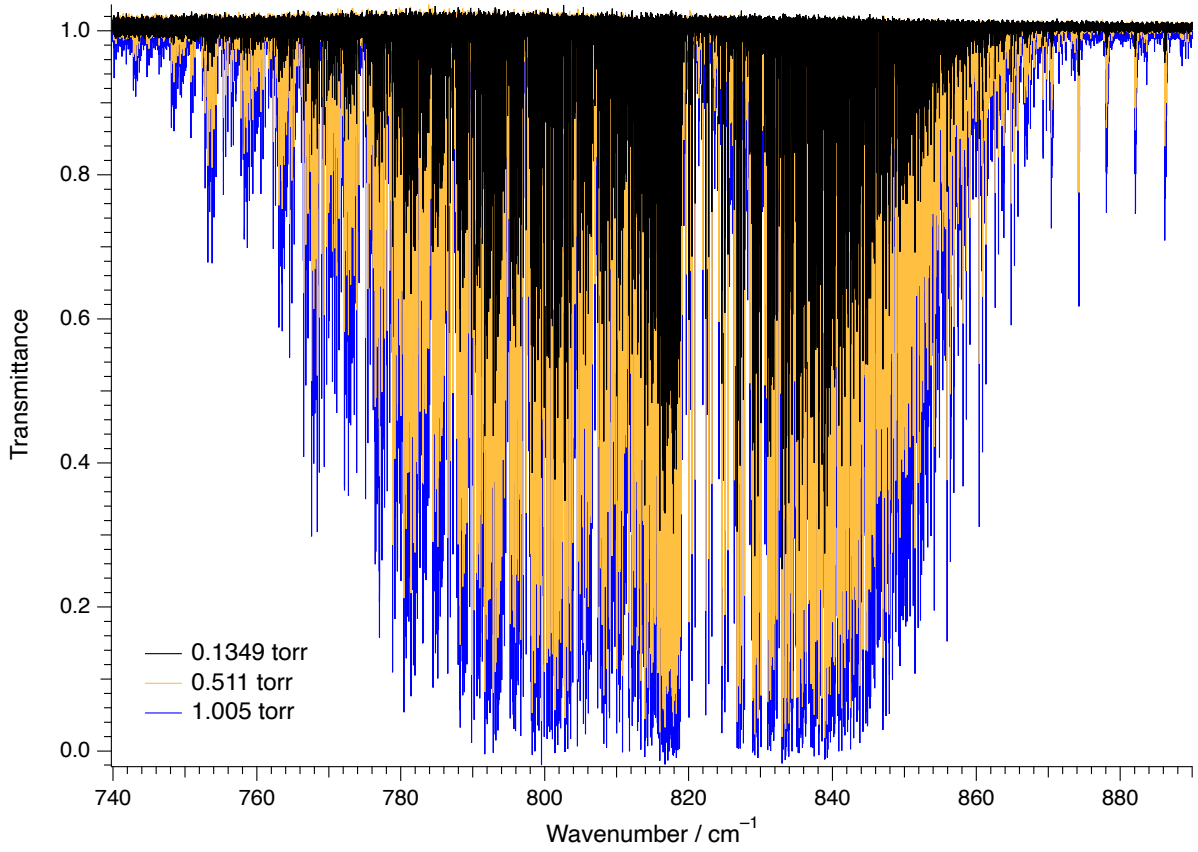

Figure 1: Overview of the high resolution (0.0019 cm^{-1}) spectrum of the ν_4 band of a sample of germane in natural isotopic abundance. The temperature and absorption path length were 300 K and 5.1 cm, respectively. The 3 spectra presented (S1 to S3 in Table 1) were used in the present work to retrieve line intensities for that band.

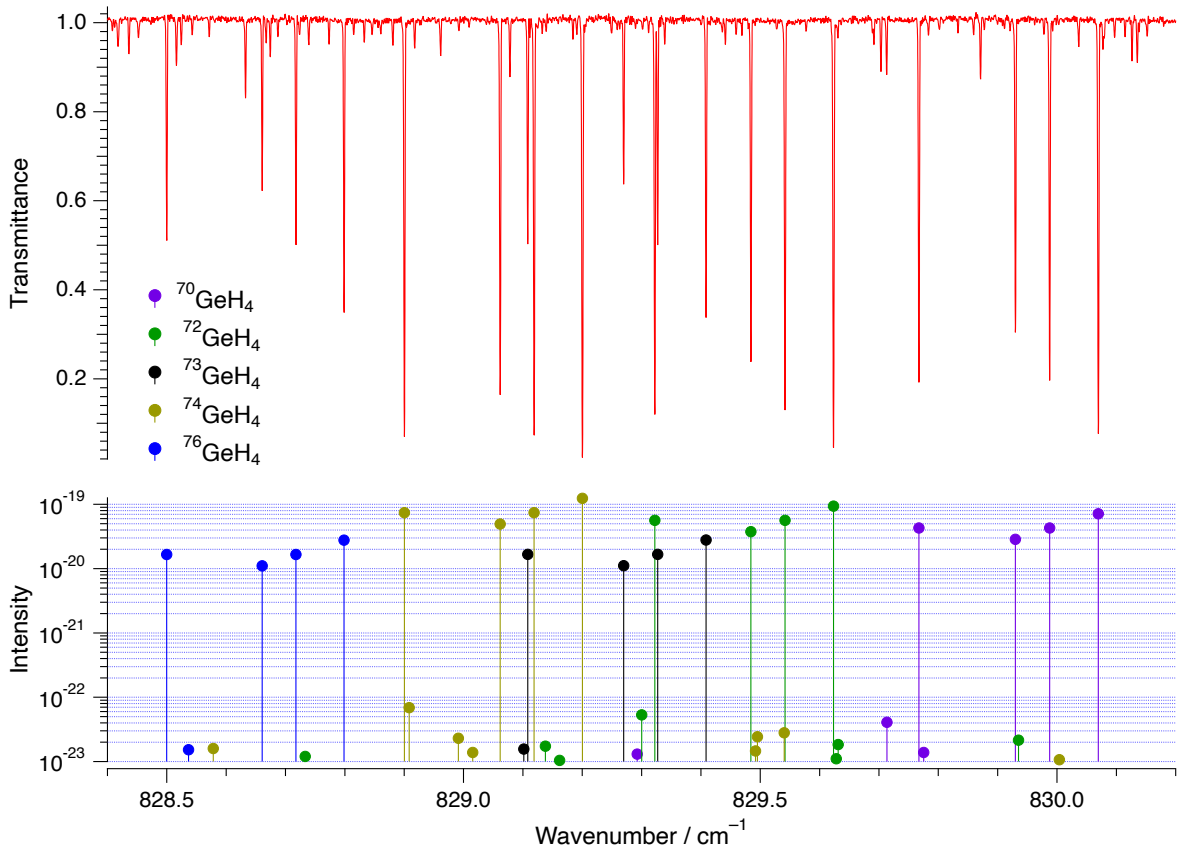

Figure 2: High resolution (0.0019 cm^{-1}) spectrum of the $R(4)$ manifold in the ν_4 band of the 5 isotopologues of germane studied in the present work. The observed spectrum is presented in the upper panel (S2 in Table 1). The lower panel displays the integrated absorption cross sections of the lines of the various isotopologues [in cm^{-1}/(molecule cm^{-2}) at 300 K], predicted by the theoretical model.

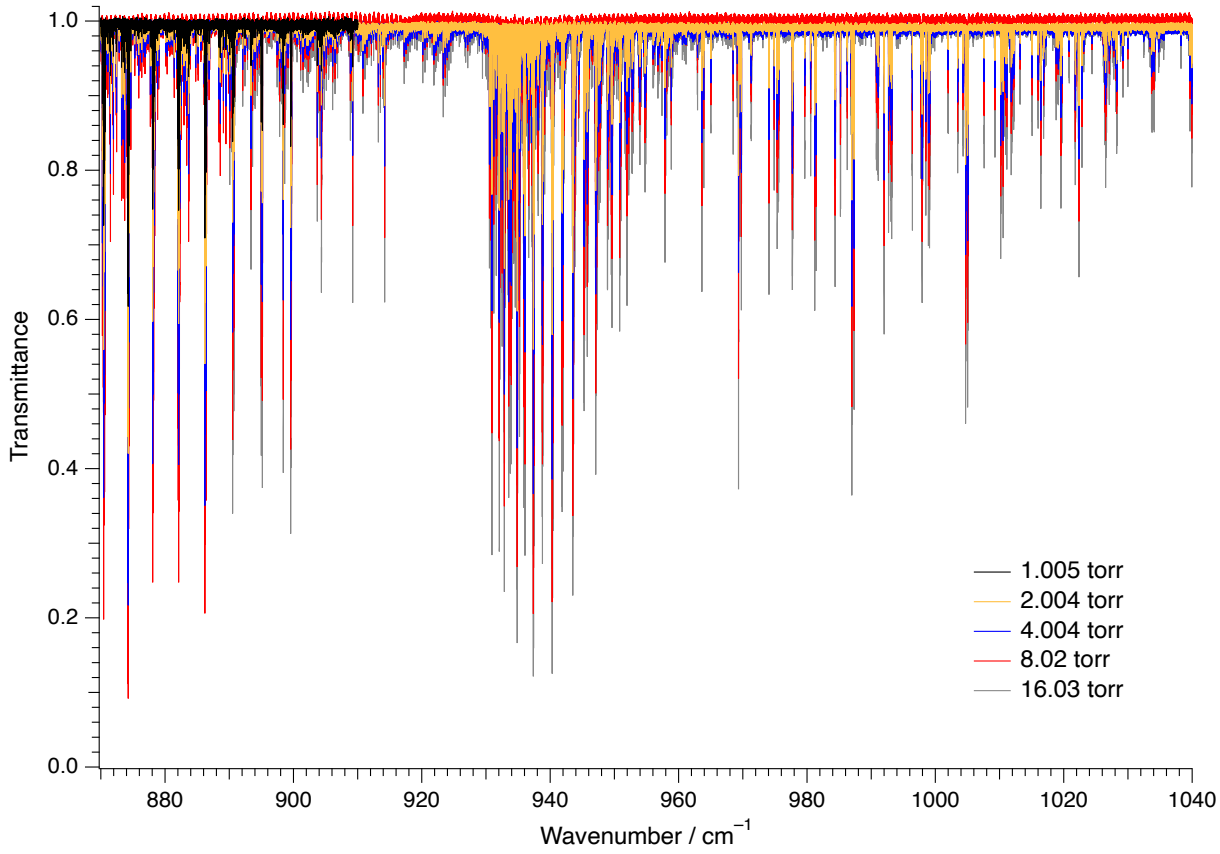

Figure 3: Overview of the high resolution (0.0019 cm^{-1}) spectrum of the ν_2 band of a sample of germane in natural isotopic abundance. The temperature and absorption path length were and 300 K and 5.1 cm, respectively. The 5 spectra presented (S3 to S7 in Table 1) were used in the present work to retrieve line intensities for that band.

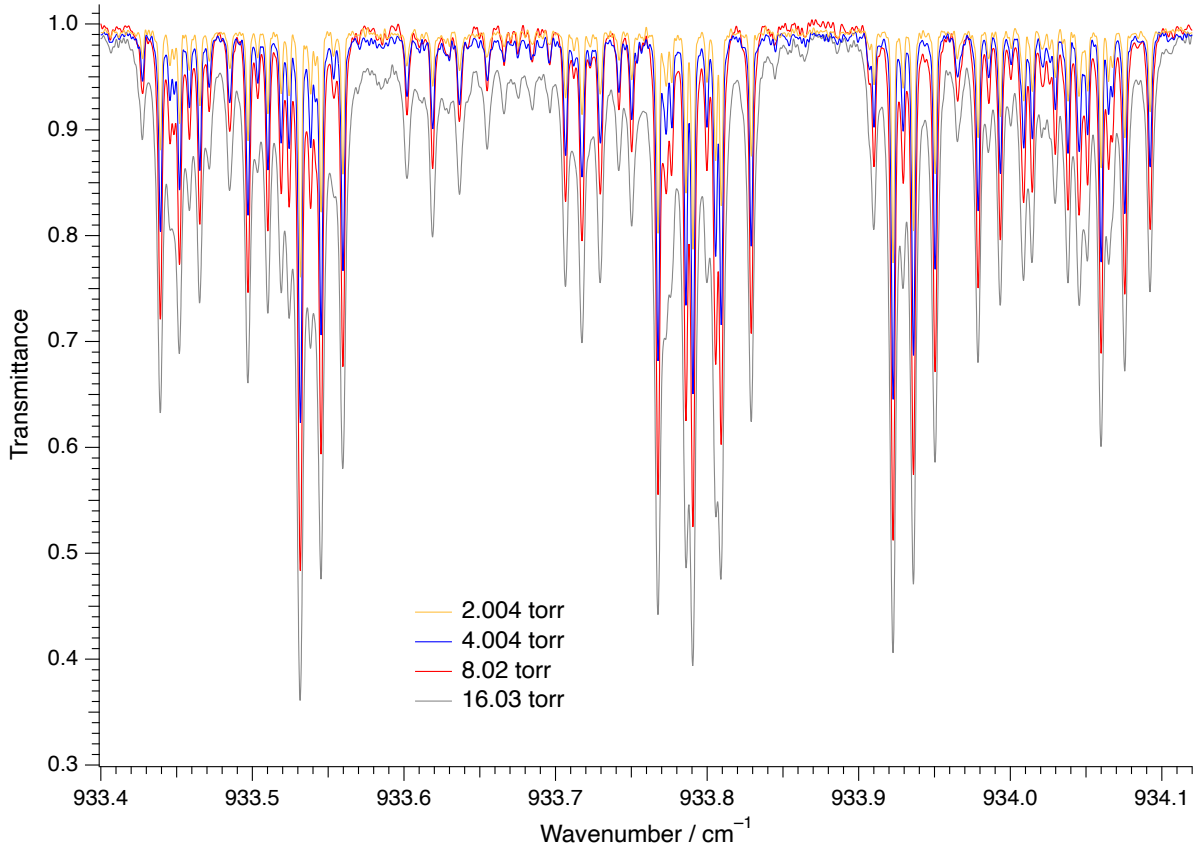

Figure 4: Same as Fig. 3 (upper panel), showing a small part of the Q branch of the ν_2 band of the 5 isotopologues of germane studied in the present work.

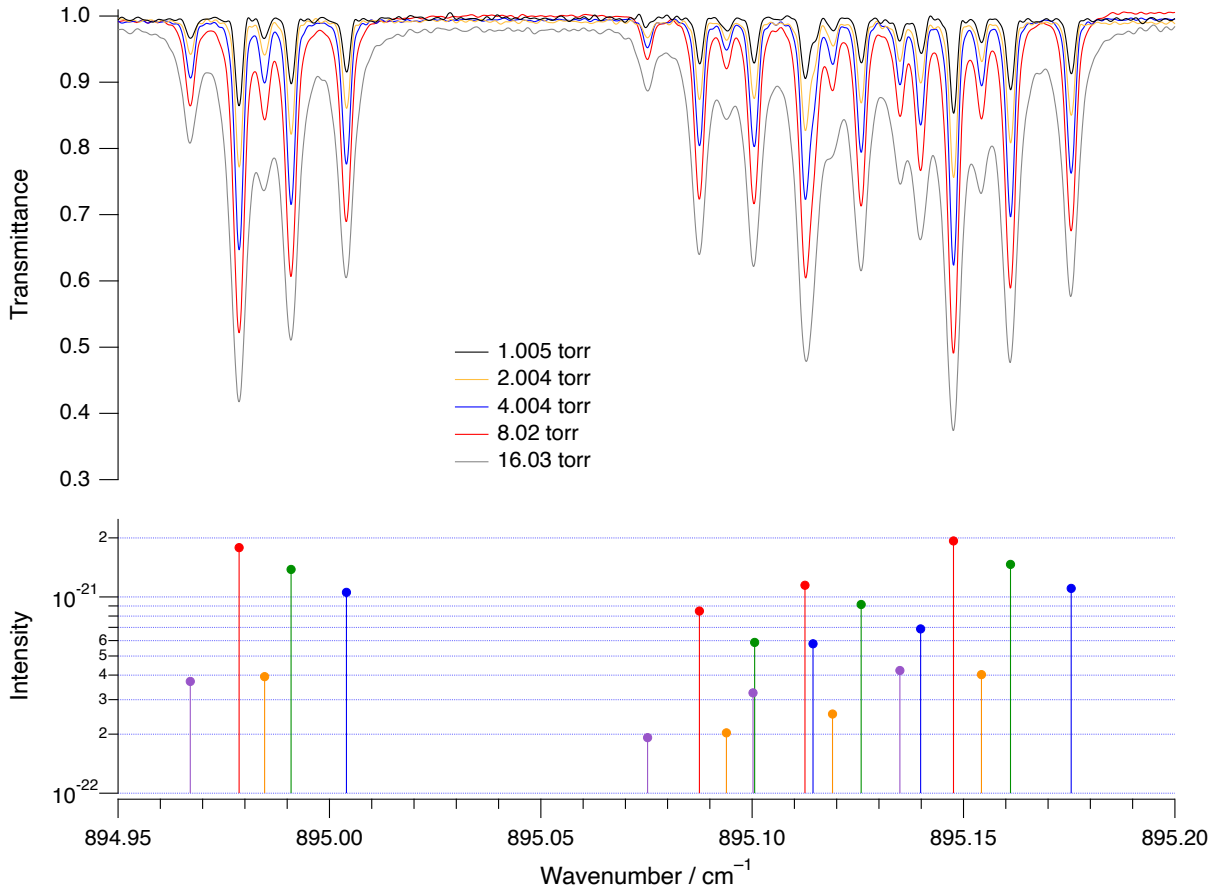

Figure 5: High resolution (0.0019 cm^{-1}) spectra of a small part of the P branch of the ν_2 band of the 5 isotopologues of germane studied in the present work, showing the increase with pressure of the spectral congestion. The lower panel displays the integrated absorption cross sections of the lines of the various isotopologues [in cm^{-1}/(molecule cm^{-2}) at 300 K], predicted by the theoretical model (blue: $^{70}GeH_4$; green: $^{72}GeH_4$; orange: $^{73}GeH_4$; red: $^{74}GeH_4$; violet: $^{76}GeH_4$).

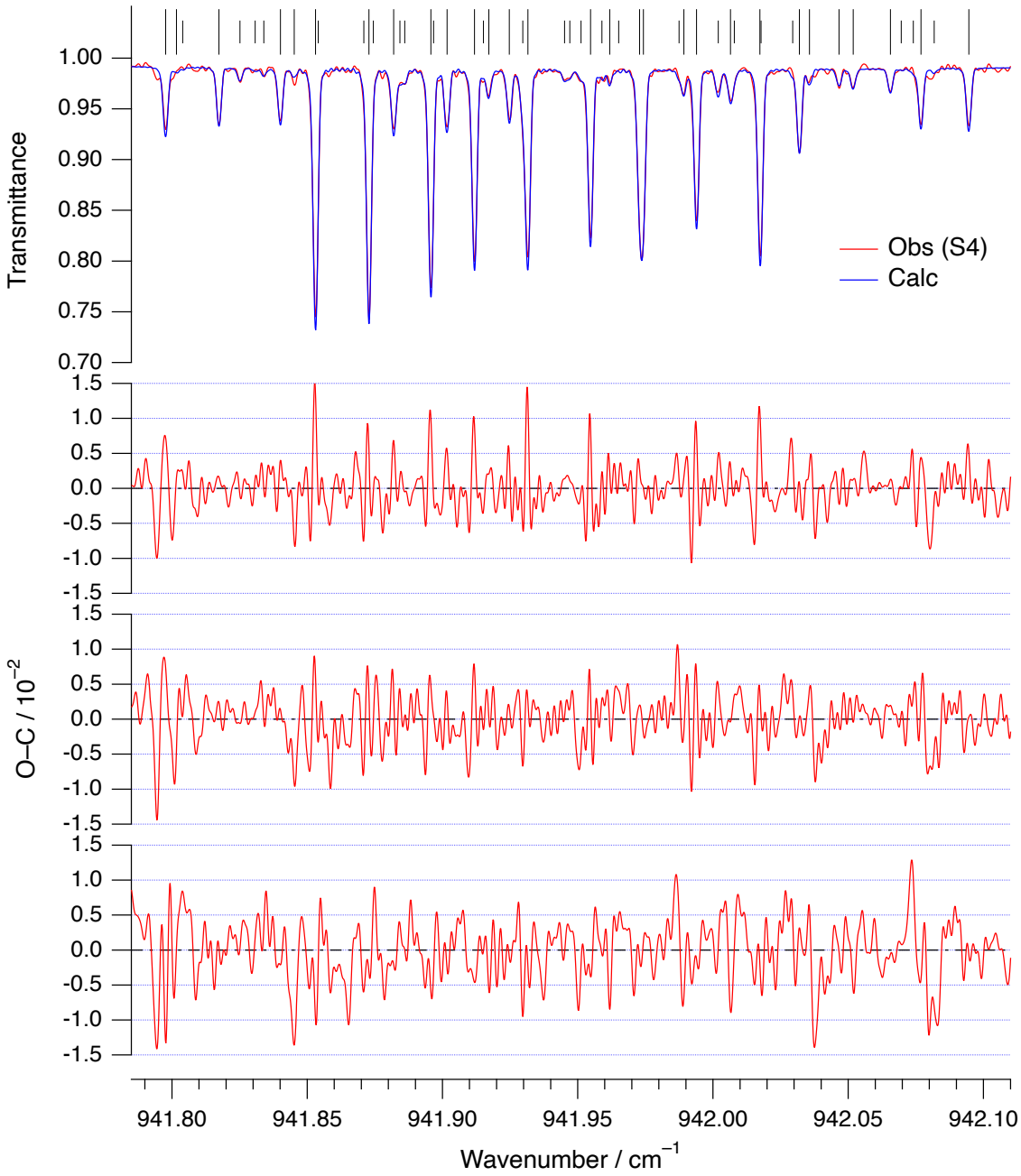

Figure 6: Results of the multi-spectrum analysis applied to 3 spectra (S4 to S6 in Table 1) of a portion of the Q branch of the ν_2 band of germane in natural isotopic abundance: observed (spectrum S4; red) and best-fit calculated (blue) spectra (top panel), and best-fit residuals corresponding to spectra S4 to S7 (from top to bottom). The vertical bars at the top indicate the positions of the lines included in the analysis, the taller ones identifying the lines for which at least one parameter (position, intensity or self broadening coefficient) was fitted.

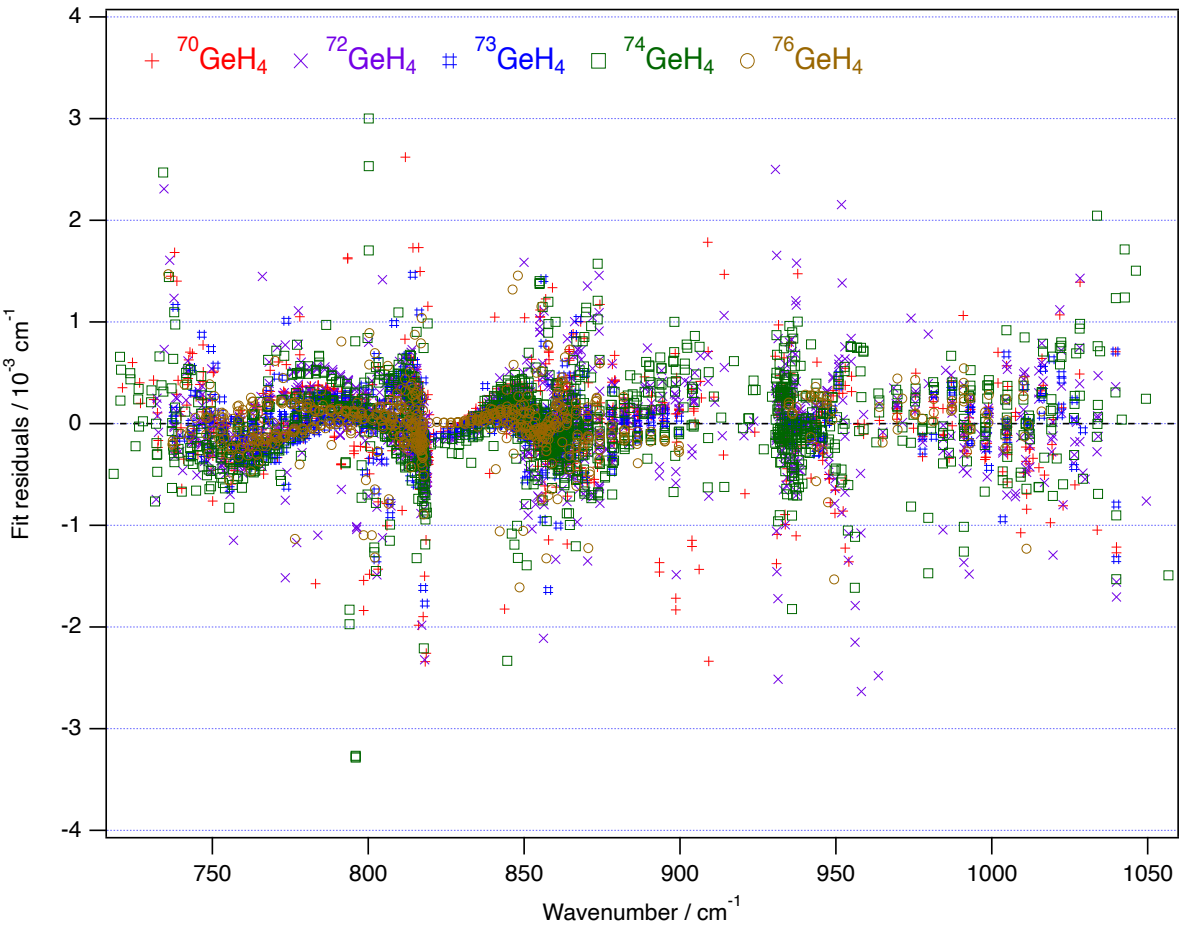

Figure 7: Fit residuals for line positions, for the five isotopologues under consideration, as a function of the wavenumber.

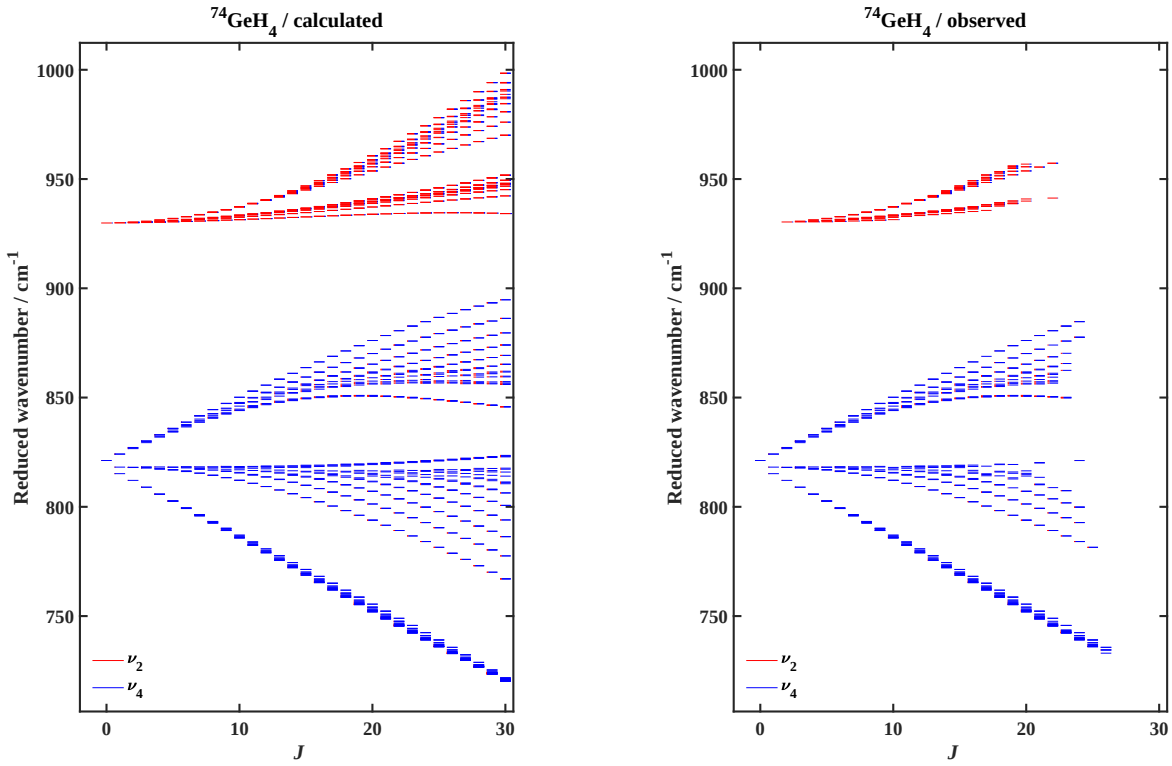

Figure 8: Calculated (left panel) and observed (right panel) reduced energy levels for $^{74}GeH_4$, as a function of the rotational quantum number J. Observed levels correspond to levels reached by assigned transitions. The colors indicate the mixings between both vibrational levels, *i.e.* the projection of each eigenlevel on the $v_2 = 1$ (red) and $v_4 = 1$ (blue) initial normal mode basis set.

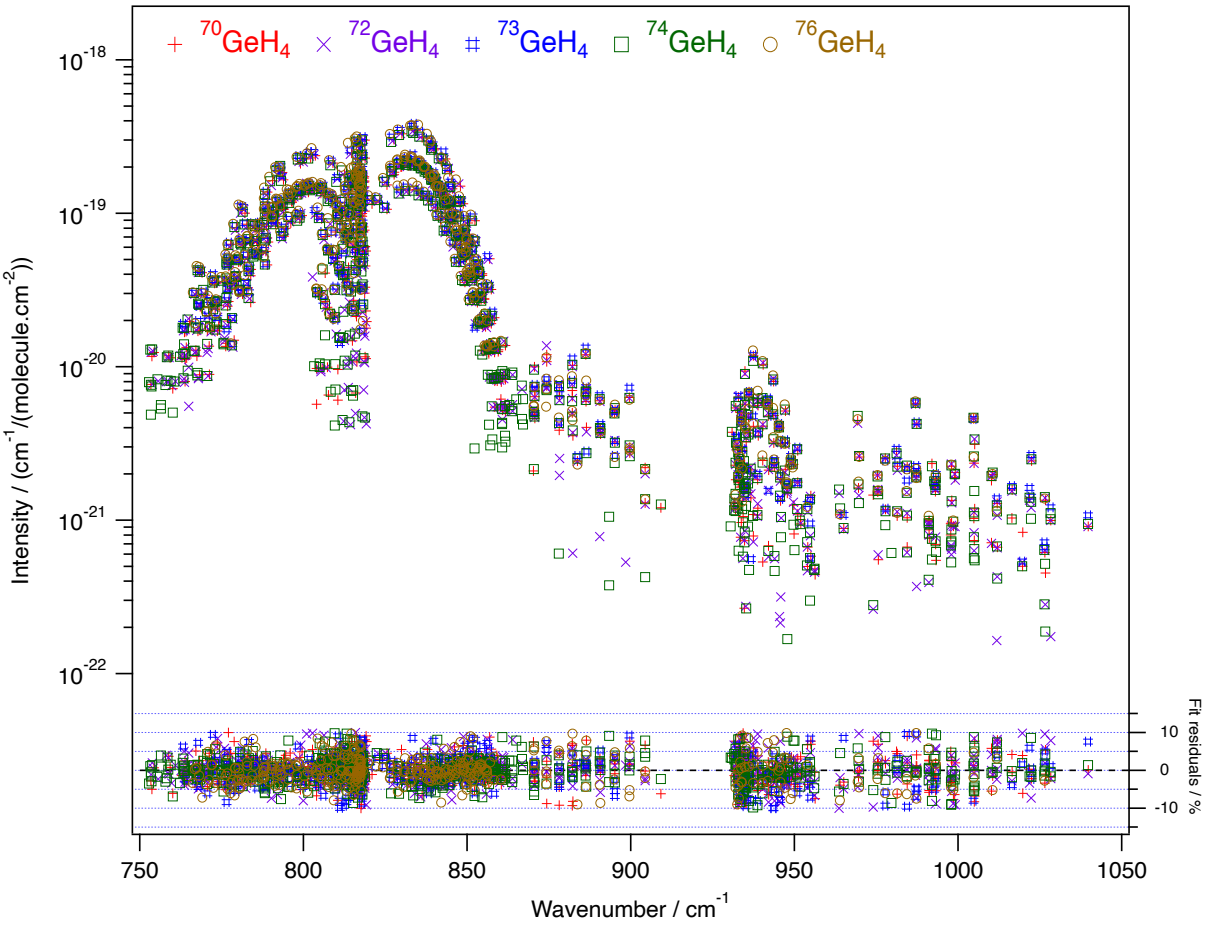

Figure 9: Line intensities for assigned lines (top panel) and relative effective dipole moment fit residuals (bottom panel), for the five isotopologues under consideration, as a function of the wavenumber.

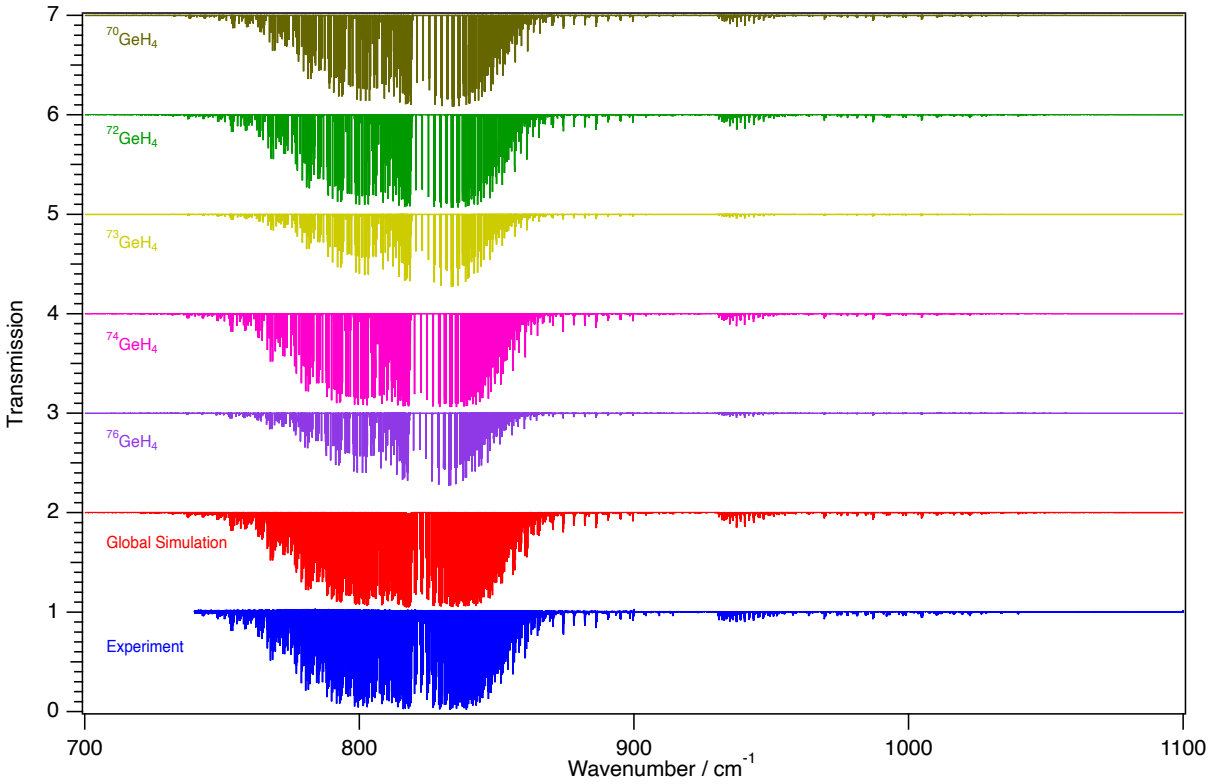

Figure 10: Spectrum simulation overview of all five germane isotopologues in natural abundance. The red curve is the total simulation including all five isotopologues. For the experimental curve (in blue), we used spectra S2 (for the ν_4 region, below 900 cm^{-1}) and S7 (for the ν_2 region, above 900 cm^{-1}) since both bands were recorded under different conditions (see Table 2). On this figure, the intensity of the S7 spectrum was multiplied by a factor 0.12 in intensity, for sake of clarity.

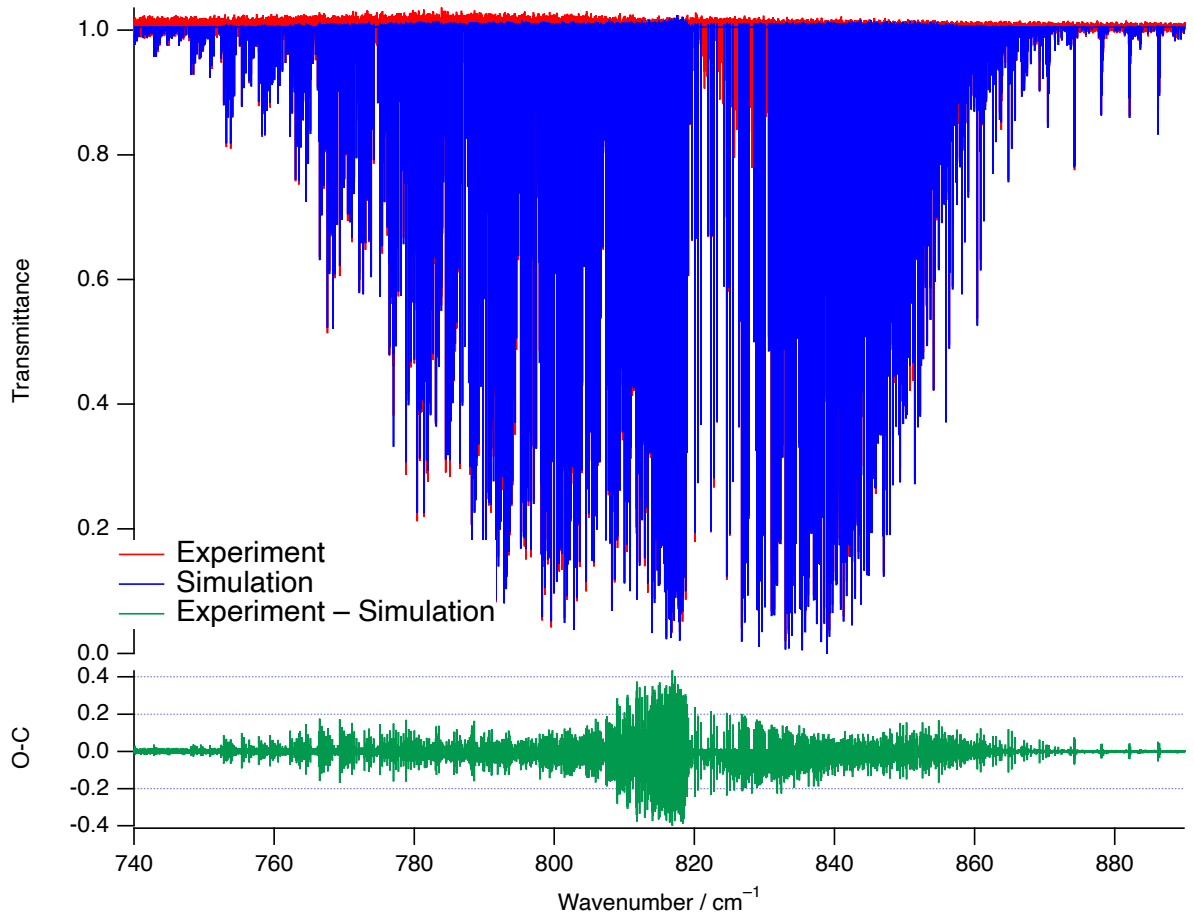

Figure 11: Comparison between experimental spectrum S2 (see Table 1) and the simulation under the same conditions (top panel) in the ν_4 region for the five isotopologues in natural abundance. The bottom panel displays the difference between these two curves.

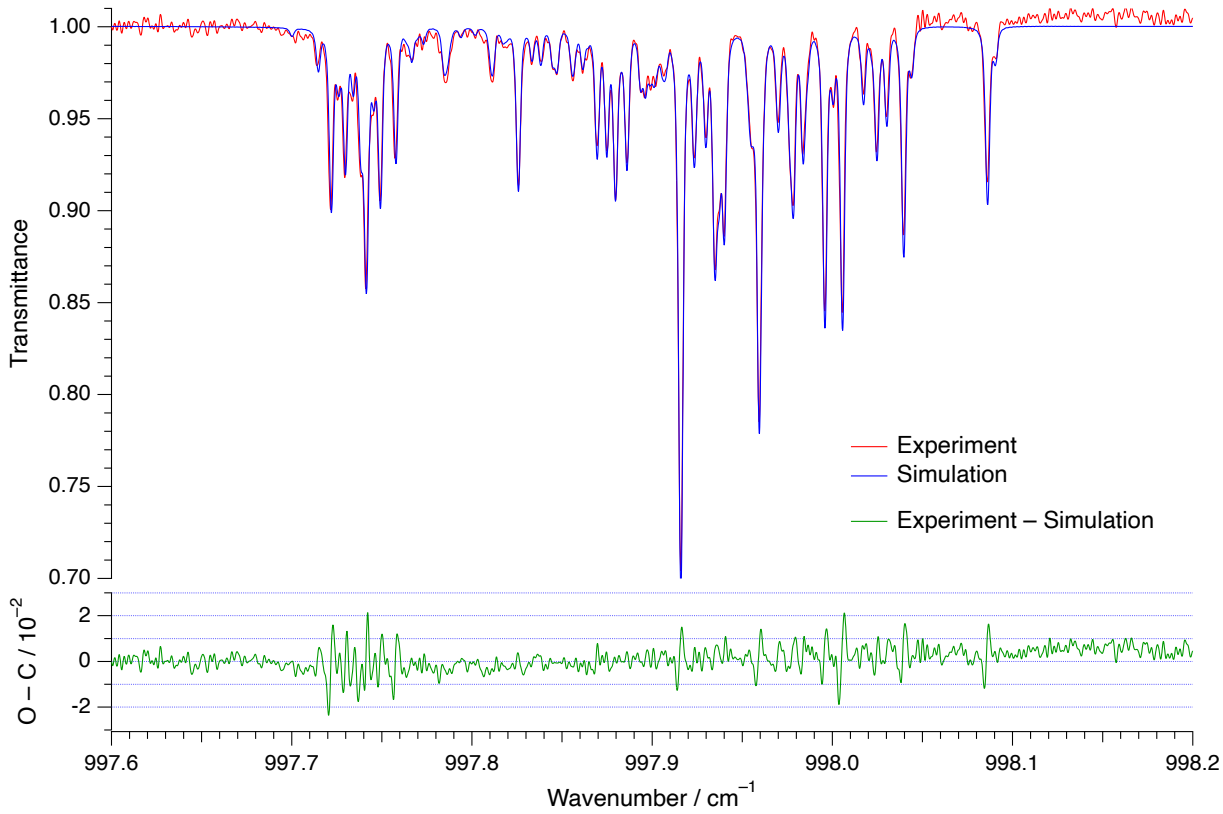

Figure 12: Comparison between experimental spectrum S6 (see Table 1) and the simulation under the same conditions (top panel) in the $R(10)/R(11)$ manifold region of the ν_2 band for the five isotopologues in natural abundance. The bottom panel displays the difference between these two curves. The simulated spectrum is calculated using a canstant baseline, set to 1.

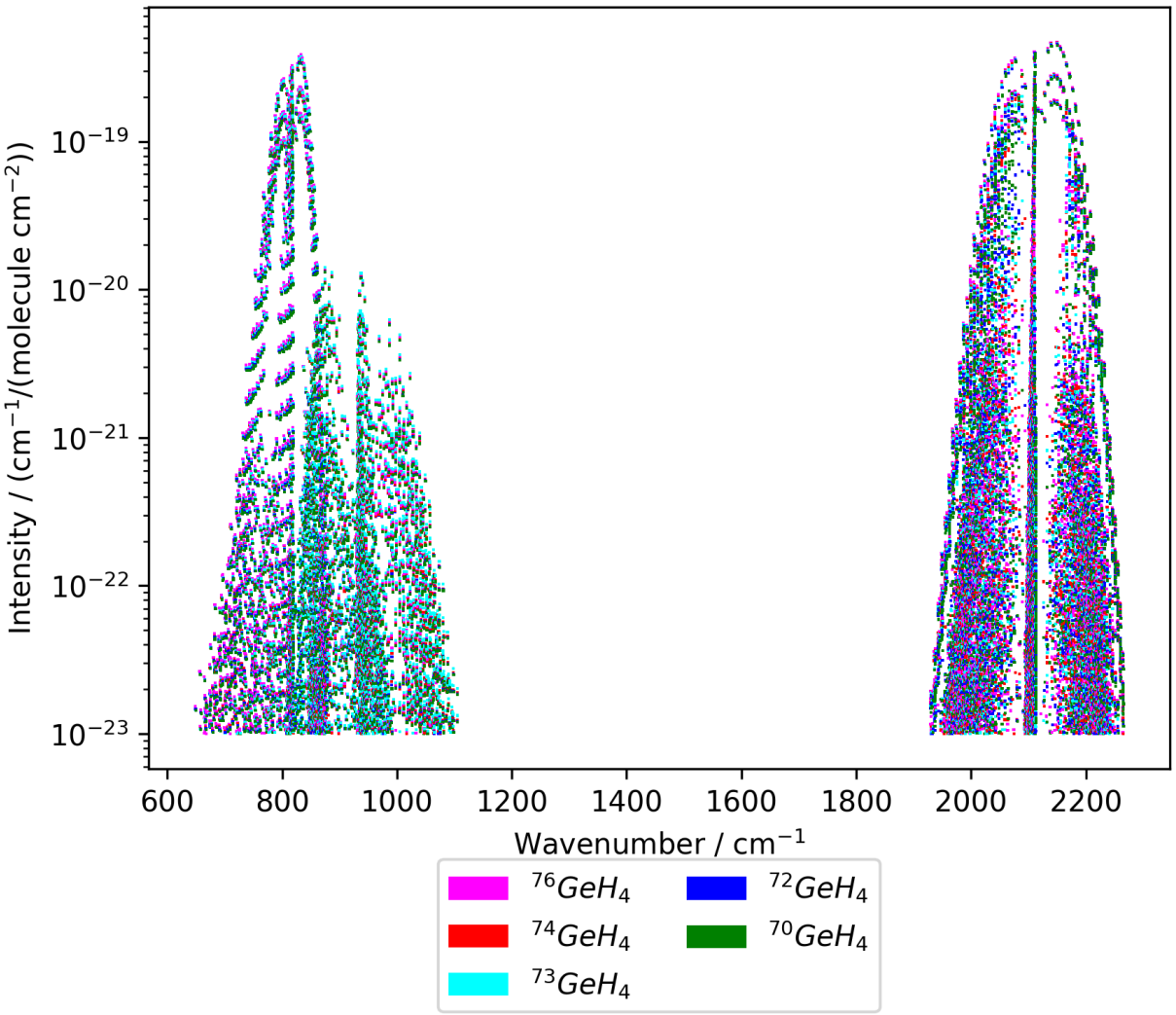

Figure 13: Extracted line by line list plotted on a graph as shown at the GeCaSDa web page (https://vamdc.icb.cnrs.fr/PHP/GeH4.php).

Tables

Table 1: Pressure of GeH_4 (in torr), spectral range recorded and number of interferograms averaged to yield the corresponding spectrum (# scans). All the spectra were recorded with an absorption path length of 5.10 ± 0.01 cm, at a stabilized room temperature of 300 ± 1 K, a resolution (equal to 0.9 divided by the maximum optical path difference) of 0.0019 cm^{-1} and an entrance aperture diameter of the interferometer equal to 1.5 mm. The absolute uncertainty on the pressure is equal to 0.5 % of the value given.

#	$P(GeH_4)$	Range / cm^{-1}	# scans
S1	0.1349 (7)	740 − 900	80
S2	0.511 (3)	740 − 890	80
S3	1.005 (5)	730 − 910	80
S4	2.004 (10)	715 − 1100	240
S5	4.004 (20)	715 − 1100	260
S6	8.02 (4)	715 − 1100	80
S7	16.03 (8)	900 − 1100	80
S8	30.07 (15)	900 − 1100	80
S9	60.05 (30)	900 − 1100	80
S10	89.97 (45)	900 − 1100	240

Table 2: Effective Hamiltonian parameters for the ground vibrational state, $v_2 = 1$ and $v_4 = 1$ levels of all five isotopologues of germane. Standard deviation is indicated in parenthesis, in the unit of last two digits.

Vibrational level ($\widetilde{H}$) or Transition ($\widetilde{\mu}$)	Order	$\Omega(K, nC)$	$\{s\}$ C_1	$\{s'\}$ C_2	Value / cm^{-1} (Hamiltonian $\widetilde{H}$) or Value / Debye (dipole moment $\widetilde{\mu}$)						Notation of Robiette *et al.* (when defined)
					$^{70}GeH_4$	$^{72}GeH_4$	$^{73}GeH_4$	$^{74}GeH_4$	$^{76}GeH_4$		
GS	0	$2(0, 0A_1)$	$0000A_1$	$0000A_1$				2.6958644 †			B_0
GS	2	$4(0, 0A_1)$	$0000A_1$	$0000A_1$				−3.3418 †		$\times 10^{-5}$	$-D_0$
GS	2	$4(4, 0A_1)$	$0000A_1$	$0000A_1$				−1.5464 †		$\times 10^{-6}$	$-\left(\sqrt{15}/4\sqrt{2}\right) D_{0t}$
GS	4	$6(0, 0A_1)$	$0000A_1$	$0000A_1$				1.142 †		$\times 10^{-9}$	H_0
GS	4	$6(4, 0A_1)$	$0000A_1$	$0000A_1$				−4.97 †		$\times 10^{-11}$	$\left(3\sqrt{5}/16\sqrt{2}\right) H_{4t}$
GS	4	$6(6, 0A_1)$	$0000A_1$	$0000A_1$				−1.600 †		$\times 10^{-11}$	$-\left(\sqrt{231}/64\sqrt{2}\right) H_{4t}$
$v_2 = 1$	0	$0(0, 0A_1)$	$0100E$	$0100E$	929.90124(19)	929.90513(17)	929.90728(48)	929.90910(15)	929.91308(44)		ν_2
$v_2 = 1$	2	$2(0, 0A_1)$	$0100E$	$0100E$	5.25(30)	5.48(32)	4.80(69)	5.32(22)	4.62(68)	$\times 10^{-3}$	$B_2 - B_0$
$v_2 = 1$	2	$2(2, 0E)$	$0100E$	$0100E$	−6.08(26)	−5.88(28)	−6.47(61)	−6.01(19)	−6.64(60)	$\times 10^{-3}$	$\sqrt{3}b_2 + 24\left(\sqrt{3}/7\right) C_6$
$v_2 = 1$	3	$3(3, 0A_2)$	$0100E$	$0100E$	−2.542(99)	−2.60(11)	−2.41(18)	−2.527(78)	−2.26(21)	$\times 10^{-5}$	$(1/2)\, d_2$
$v_2 = 1$	4	$4(0, 0A_1)$	$0100E$	$0100E$	7.92(32)	7.48(28)	7.55(19)	7.64(22)	9.07(76)	$\times 10^{-7}$	$-(D_2 - D_0)$
$v_2 = 1$	4	$4(2, 0E)$	$0100E$	$0100E$	−9.06(29)	−8.77(26)	−8.75‡	−8.75(19)	−0.996(70)	$\times 10^{-7}$	$-(3/4)\, C_5 + (9/7)\, C_6$
$v_2 = 1$	4	$4(4, 0A_1)$	$0100E$	$0100E$	6.6(1.2)	5.1(1.0)	5.91‡	5.91(85)	1.03(29)	$\times 10^{-8}$	$-\left(\sqrt{15}/4\right)(D_{2t} - D_{1t})$
$v_2 = 1$	4	$4(4, 0E)$	$0100E$	$0100E$	0.0‡	0.0‡	0.0‡	0.0‡	0.0‡		$-\left(3\sqrt{3/7}\right) C_6$
$v_2 = 1/v_4 = 1$ int.	1	$1(1, 0F_1)$	$0100E$	$0001F_2$	−4.223(17)	−4.205(18)	−4.242(39)	−4.210(13)	−4.246(39)		$-\left(\sqrt{3}\right) R_{24} + \left(\sqrt{3}/10\right) F_{24b}$
$v_2 = 1/v_4 = 1$ int.	2	$2(2, 0F_2)$	$0100E$	$0001F_2$	−2.338(30)	−2.365(32)	−2.294(73)	−2.353(22)	−2.288(68)	$\times 10^{-2}$	(undefined)
$v_2 = 1/v_4 = 1$ int.	3	$3(1, 0F_1)$	$0100E$	$0001F_2$	−1.146(10)	−1.152(13)	−1.115(37)	−1.1502(81)	−1.156(26)	$\times 10^{-4}$	$(3/4)\, R_{24}^{01} + (3/4)\, F_{24a} + (9/80)\, F_{24b}$
$v_2 = 1/v_4 = 1$ int.	3	$3(3, 0F_1)$	$0100E$	$0001F_2$	3.68(12)	3.51(11)	3.64(12)	3.536(81)	3.98(28)	$\times 10^{-5}$	$-\left(\sqrt{3}/4\sqrt{10}\right) F_{24b}$
$v_2 = 1/v_4 = 1$ int.	3	$3(3, 0F_2)$	$0100E$	$0001F_2$	2.755(72)	2.774(69)	2.89(12)	2.750(54)	2.57(20)	$\times 10^{-5}$	$\left(\sqrt{3}/2\sqrt{2}\right) F_{24c}$
$v_2 = 1/v_4 = 1$ int.	4	$4(4, 0F_1)$	$0100E$	$0001F_2$	2.33(22)	2.13(21)	2.03(23)	2.11(18)	2.96(55)	$\times 10^{-7}$	(undefined)
$v_4 = 1$	0	$0(0, 0A_1)$	$0001F_2$	$0001F_2$	821.54462(13)	821.11703(13)	820.91126(15)	820.71165(12)	820.32666(16)		ν_4
$v_4 = 1$	1	$1(1, 0F_1)$	$0001F_2$	$0001F_2$	6.36580(32)	6.37276(34)	6.37698(73)	6.37978(23)	6.38703(72)		$3\sqrt{2}\ B\zeta_4$ (ν_4 Coriolis)
$v_4 = 1$	2	$2(0, 0A_1)$	$0001F_2$	$0001F_2$	−2.42(20)	−2.58(21)	−2.13(46)	−2.49(15)	−2.02(46)	$\times 10^{-3}$	$B_4 - B_0$
$v_4 = 1$	2	$2(2, 0E)$	$0001F_2$	$0001F_2$	3.72(30)	3.96(32)	3.29(69)	3.82(22)	3.13(69)	$\times 10^{-3}$	$-(1/2)\alpha_{220} - 6\alpha_{224}$
$v_4 = 1$	2	$2(2, 0F_2)$	$0001F_2$	$0001F_2$	−1.479(23)	−1.496(24)	−1.444(52)	−1.483(17)	−1.429(52)	$\times 10^{-2}$	$-(3/4)\alpha_{220} + 6\alpha_{224}$
$v_4 = 1$	3	$3(1, 0F_1)$	$0001F_2$	$0001F_2$	1.401(15)	1.409(16)	1.383(26)	1.399(12)	1.362(32)	$\times 10^{-4}$	$-(3(\sqrt{3})/4(\sqrt{2})F_{110}$
$v_4 = 1$	3	$3(3, 0F_1)$	$0001F_2$	$0001F_2$	1.75(12)	1.80(13)	1.56(24)	1.707(97)	1.41(27)	$\times 10^{-5}$	$(3/\sqrt{5}/2)F_{134}$
$v_4 = 1$	4	$4(0, 0A_1)$	$0001F_2$	$0001F_2$	−1.140(23)	−1.113(21)	−1.1113(95)	−1.116(16)	−1.212(53)	$\times 10^{-6}$	$-(D_4 - D_0)$
$v_4 = 1$	4	$4(2, 0E)$	$0001F_2$	$0001F_2$	−3.91(12)	−3.75(11)	−3.728(47)	−3.797(83)	−4.29(28)	$\times 10^{-7}$	$\left(\sqrt{3}/8\right) G_{220} + \left(3\sqrt{3}/2\right) G_{224}$
$v_4 = 1$	4	$4(4, 0A_1)$	$0001F_2$	$0001F_2$	−1.15(10)	−1.038(89)	−1.055(22)	−1.070(71)	−1.45(24)	$\times 10^{-7}$	$\left(3\sqrt{3}/16\right) G_{220} - \left(3\sqrt{3}/2\right) G_{224}$
$v_4 = 1$	4	$4(4, 0E)$	$0001F_2$	$0001F_2$	−3.43(34)	−3.06(30)	−3.15‡	−3.15(23)	−4.36(83)	$\times 10^{-7}$	$\left(-3\sqrt{5}/4\sqrt{2}\right)(D_{4t} - D_{0t})$
$v_4 = 1$	5	$5(1, 0F_1)$	$0001F_2$	$0001F_2$	1.344(83)	1.236(87)	1.43(17)	1.198(73)	0.99(19)	$\times 10^{-9}$	$\left(-3\sqrt{7}/2\right) G_{244} + \left(\sqrt{21}/2\sqrt{22}\right) G_{246}$
$v_4 = 1$	5	$5(3, 0F_1)$	$0001F_2$	$0001F_2$	−1.698(72)	−1.886(69)	−1.79(13)	−1.903(62)	−1.87(12)	$\times 10^{-9}$	$\left(-9\sqrt{7}/8\right) G_{244} - \left(\sqrt{21}/\sqrt{22}\right) G_{246}$
Abundance / %					21.23	27.66	7.73	35.94	7.44		
Nb. data					1031	1187	603	1394	638		
J_{max}					26	26	23	25	24		
d_{RMS}*					0.458	0.475	0.310	0.486	0.303		

† Ground state parameters are fixed to $^{74}GeH_4$ values from the previous study of the ν_1/ν_3 stretching dyad.

‡ Fixed value.

* $d_{RMS}/10^{-3}$cm^{-1}.

Table 3: Effective dipole moment parameter values for the ν_2 and ν_4 bands of all five germane isotopologues. Standard deviation is indicated in parenthesis, in the unit of last two digits.

Band	Order	$\Omega(K,nC)$	$\{s\}$ C_1	$\{s'\}$ C_2	Value / Debye						Description
					$^{70}GeH_4$	$^{72}GeH_4$	$^{73}GeH_4$	$^{74}GeH_4$	$^{76}GeH_4$		(when available, see Eq. (6))
ν_2	1	$1(1,0F_1)$	$0000A_1$	$0100E$	−6.0723(16)	−6.1851(17)	−6.5380(17)	−6.2307(19)	−5.5405(16)	$\times10^{-4}$	μ_2^1
ν_4	0	$0(0,0A_1)$	$0000A_1$	$0001F_2$	3.44763(13)	3.46372(17)	3.567616(64)	3.48751(22)	3.629326(63)	$\times10^{-1}$	$\mu_4^0 = \left(\sqrt{3/2}\right)(\partial\mu_4/\partial q_4)_0$
ν_4	1	$1(1,0F_1)$	$0000A_1$	$0001F_2$	−2.1005(53)	−2.0749(63)	−2.1678(33)	−1.8940(76)	−2.2371(33)	$\times10^{-4}$	μ_4^1 = Herman-Wallis factor
ν_4	2	$2(0,0A_1)$	$0000A_1$	$0001F_2$	−3.4521(34)	−3.6715(40)	−3.1972(23)	−3.7483(48)	−3.12063(23)	$\times10^{-5}$	μ_4^2
Abundance / %					21.23	27.66	7.73	35.94	7.44		
Nb. data					573	620	389	666	372		
J_{max}					23	21	20	21	19		
$d_{RMS}/\%$					3.488	3.512	3.925	3.358	3.689		

Table 4: Rovibrational transitions in GeCaSDa. The polyad sheme is described by the (i_1, i_2, i_3, i_4) multiplet as explained in Section 2 of Ref. [34].

Transitions	Nb. dipolar	Dipolar wavenumber cm^{-1}	Dipolar intensity $cm^{-1}/(molecule\ cm^{-2})$
$^{70}GeH_4$			
Scheme 1 (1,0,1,0)			
$P_1 - P_0$	6426	1930 – 2270	8×10^{-24} – 4×10^{-19}
Scheme 2 (0,1,0,1)			
$P_1 - P_0$	5666	650 – 1106	8×10^{-24} – 4×10^{-19}
$^{72}GeH_4$			
Scheme 1 (1,0,1,0)			
$P_1 - P_0$	6462	1930 – 2270	8×10^{-24} – 4×10^{-19}
Scheme 2 (0,1,0,1)			
$P_1 - P_0$	5679	649 – 1106	8×10^{-24} – 4×10^{-19}
$^{73}GeH_4$			
Scheme 1 (1,0,1,0)			
$P_1 - P_0$	6470	1929 – 2270	8×10^{-24} – 4×10^{-19}
Scheme 2 (0,1,0,1)			
$P_1 - P_0$	5700	649 – 1105	8×10^{-24} – 4×10^{-19}
$^{74}GeH_4$			
Scheme 1 (1,0,1,0)			
$P_1 - P_0$	6509	1929 – 2270	8×10^{-24} – 4×10^{-19}
Scheme 2 (0,1,0,1)			
$P_1 - P_0$	5700	649 – 1105	8×10^{-24} – 4×10^{-19}
$^{76}GeH_4$			
Scheme 1 (1,0,1,0)			
$P_1 - P_0$	6525	1929 – 2269	8×10^{-24} – 4×10^{-19}
Scheme 2 (0,1,0,1)			
$P_1 - P_0$	5741	648 – 1105	8×10^{-24} – 4×10^{-19}
Total	60 878		